

The spindle assembly checkpoint (SAC) monitors and promotes kinetochore-microtubule attachment during mitosis. Bub1 and BubR1, SAC components, originated from duplication of an ancestor gene. Subsequent sub-functionalization established subordination: Bub1, recruited first to kinetochores, promotes successive BubR1 recruitment. Because both Bub1 and BubR1 heterodimerize with Bub3, a targeting adaptor for phosphorylated kinetochores, the molecular basis for such sub-functionalization is unclear. We demonstrate that Bub1, but not BubR1, enhances binding of Bub3 to phosphorylated kinetochores. Grafting a short motif of Bub1 onto BubR1 promotes Bub1-independent kinetochore recruitment of BubR1. Such gain-of-function BubR1 mutant cannot sustain a functional checkpoint. We demonstrate that kinetochore localization of BubR1 relies on direct hetero-dimerization with Bub1 at a pseudo-symmetric interface. Such pseudo-symmetric interaction underpins a template-copy relationship crucial for kinetochore-microtubule attachment and SAC signaling. Our results illustrate how gene duplication and sub-functionalization shape the workings of an essential molecular network.

Introduction

Bub1 and BubR1 are paralogous proteins involved in the spindle assembly checkpoint (SAC), a safety device that monitors the attachment of kinetochores to spindle microtubules and halts mitotic progression until completion of chromosome bi-orientation on the mitotic spindle (Foley and Kapoor, 2013; Lara-Gonzalez et al., 2012). Bub1 and BubR1 originated from a gene that was already present in the hypothetical last eukaryotic common ancestor (LECA) (Suijkerbuijk et al., 2012a). After speciation, up to nine distinct duplication events might have occurred, which invariably led to sub-functionalization of the resulting gene products (Suijkerbuijk et al., 2012a).

56 Human Bub1 and BubR1 are strongly conserved at the sequence and domain level
57 (Figure 1A), but play complementary roles in the SAC. Bub1 becomes recruited to
58 kinetochores in prometaphase to provide a platform for additional SAC proteins,
59 including Mad1, Mad2, the BubR1/Bub3 complex and Cdc20. Bub1 promotes the
60 assembly of a subset of these proteins, Mad2, BubR1/Bub3 and Cdc20, into the SAC
61 effector, the mitotic checkpoint complex (MCC), which targets the anaphase promoting
62 complex/cyclosome (APC/C) to inhibit its ability to promote mitotic exit (Foley and
63 Kapoor, 2013; Lara-Gonzalez et al., 2012). Bub1, not in itself an MCC subunit, likely
64 catalyzes MCC assembly by aligning MCC subunits for a profitable interaction (discussed
65 in Overlack et al., 2014). Bub1 kinase activity is not required for the SAC (Fernius and
66 Hardwick, 2007; Klebig et al., 2009; Perera et al., 2007; Sharp-Baker and Chen, 2001), but
67 contributes to stable kinetochore-microtubule attachments through phosphorylation of
68 histone H2A on Thr120 and subsequent localization of Sgo1 to centromeres and
69 kinetochores (Caldas et al., 2013; Kawashima et al., 2010; Wang et al., 2011). BubR1, on
70 the other hand, evolved into an inactive pseudo-kinase (Suijkerbuijk et al., 2012a) and is a
71 crucial subunit of the MCC (Fraschini et al., 2001; Hardwick et al., 2000; Sudakin et al.,
72 2001). BubR1 contributes to the formation of stable kinetochore-microtubule
73 attachments and checkpoint silencing through kinetochore co-recruitment of protein
74 phosphatase 2A (PP2A) (Kruse et al., 2013; Suijkerbuijk et al., 2012b; Xu et al., 2013;
75 Espert et al., 2014; Nijenhuis et al. 2014).

76 Bub1 and BubR1 have different kinetochore dynamics, likely reflecting their distinct
 77 functions in the SAC. Bub1 interacts stably with unattached kinetochores, in agreement
 78 with its function as a SAC recruitment platform, while BubR1 turns over rapidly ($t_{1/2} =$
 79 3-20 s), likely reflecting its cycle of incorporation into MCC and its release into the
 80 cytosol as a soluble APC/C inhibitor (Howell et al., 2004; Shah et al., 2004). Besides
 81 different dynamics, another important difference is that kinetochore recruitment of Bub1
 82 is independent of BubR1, while recruitment of BubR1 is strictly subordinate to Bub1
 83 (Gillett et al., 2004; Johnson et al., 2004; Klebig et al., 2009; Logarinho et al., 2008;
 84 Millband and Hardwick, 2002; Perera et al., 2007). The molecular basis for these
 85 differences is unclear, because both Bub1 and BubR1 bind a kinetochore-targeting
 86 adaptor named Bub3. Bub3 is a 7-WD40 β -propeller that targets kinetochores by binding
 87 to phosphorylated Met-Glu-Leu-Thr^P (MELT^P, where T^P indicates phosphothreonine)
 88 repeats of the outer kinetochore subunit Knl1 (a.k.a. Casc5, Spc105, Spc7, AF15q14, and
 89 Blinkin) (Kiyomitsu et al., 2007; Krenn et al., 2014; 2012; London et al., 2012; Primorac
 90 et al., 2013; Shepperd et al., 2012; Yamagishi et al., 2012) (Figure 1B). Bub3 binds tightly
 91 to Bub1 and BubR1 via conserved segments known as Bub3-binding domain (B3BD) or
 92 GLEBS (Larsen et al., 2007; Taylor et al., 1998). By recognizing MELT^P, Bub3 co-
 93 recruits Bub1 to kinetochores in *S. cerevisiae* (Primorac et al., 2013). In human cells, Bub3
 94 is required for kinetochore recruitment of Bub1 and BubR1, and consistently the B3BDs
 95 of Bub1 and BubR1 are necessary, and in the case of Bub1 also sufficient, for

kinetochore targeting of Bub1 and BubR1 (Elowe et al., 2010; Krenn et al., 2012; Lara-Gonzalez et al., 2011; Logarinho et al., 2008; Malureanu et al., 2009; Taylor et al., 1998). The subordination of BubR1 kinetochore recruitment to the presence of Bub1 suggests that Bub3 may operate differently when bound to Bub1 or BubR1. Here, we set out to investigate the molecular basis of this phenomenon and its implications for spindle checkpoint signaling and kinetochore-microtubule attachment.

Results

Mps1 and Bub1 are required for kinetochore localization of BubR1 The SAC kinase Mps1 has been shown to phosphorylate MELT repeats of Knl1 to promote kinetochore recruitment of Bub1 and BubR1 (Krenn et al., 2014; Heinrich et al., 2012; London et al., 2012; Primorac et al., 2013; Shepperd et al., 2012; Vleugel et al., 2013; Yamagishi et al., 2012). We precipitated Bub1 or Knl1 (Vleugel et al., 2013) from mitotic lysates of HeLa cells treated with or without the Mps1 inhibitor Reversine (Santaguida et al., 2010). Quantitative mass spectrometry (see Methods) of proteins associated with Bub1 or Knl1 confirmed the crucial role of Mps1, as we observed a strong suppression of the interaction of Bub1, BubR1 and Bub3 with kinetochores in the presence of Reversine (Figure 1C-D. Large deviations from a value of 1 for the Reversine/DMSO ratio indicate suppression of binding).

In HeLa cells treated with nocodazole, which depolymerizes microtubules and activates

116 the SAC, Bub1 decorated kinetochores at essentially normal levels after depletion of
117 BubR1 (Figure 1E, quantified in Figure 1F. Quantifications of RNAi-based depletions
118 are shown in Figure 1 Supplement 1A-B). Conversely, BubR1 did not decorate
119 kinetochores after Bub1 depletion (Figure 1G-H). These results confirm that BubR1
120 requires Bub1 for kinetochore recruitment, in line with previous studies (Gillett et al.,
121 2004; Johnson et al., 2004; Klebig et al., 2009; Logarinho et al., 2008; Millband and
122 Hardwick, 2002; Perera et al., 2007).

123 By monitoring the localization of a GFP-Bub1 reporter construct, we had previously
124 demonstrated that Bub1²⁰⁹⁻²⁷⁰, encompassing the B3BD, is the minimal Bub1 localization
125 domain (Krenn et al., 2012; Taylor et al., 1998). Bub1²⁰⁹⁻²⁷⁰ targeted kinetochores very
126 efficiently even after depletion of endogenous Bub1 (Figure 1I). We asked if an
127 equivalent GFP reporter construct encompassing the B3BD of BubR1, BubR1³⁶²⁻⁴³¹, was
128 also recruited to kinetochores. BubR1³⁶²⁻⁴³¹ was not recruited to kinetochores even in the
129 presence of Bub1 (Figure 1J. Diagrams of Bub1 and BubR1 deletions used in this study
130 are in Figure 1 Supplement 1C-D). Thus, even if Bub1 and BubR1 share a related B3BD
131 to interact with the same kinetochore-targeting subunit (Bub3) and interact in a
132 phosphorylation-dependent manner with Knl1, the mechanisms of their kinetochore
133 recruitment are different. This raises two crucial questions: 1) why is the B3BD region of
134 Bub1 sufficient for kinetochore recruitment, while the equivalent region of BubR1 is
135 not? And 2) if binding to Bub3 is not sufficient for robust kinetochore recruitment of

BubR1, how is BubR1 recruited to kinetochores? We will focus sequentially on these questions.

The loop regions of Bub1 and BubR1 modulate the interaction of Bub3 with

phosphorylated MELT motifs To investigate if and how Bub1²⁰⁹⁻²⁷⁰ and BubR1³⁶²⁻⁴³¹

modulate the binding affinity of Bub3 for the MELT^P repeats of Knl1, we immobilized

on amylose beads a fusion of maltose-binding protein (MBP) with residues 138-168 of

Knl1, a region containing a single and functional MELT repeat (the most N-terminal,

and therefore called MELT1; Krenn et al., 2014). We treated MBP-Knl1^{MELT1} with or

without Mps1 kinase. Next, we incubated MBP-Knl1^{MELT1} with Bub3, Bub1²⁰⁹⁻²⁷⁰/Bub3,

or BubR1³⁶²⁻⁴³¹/Bub3, and visualized bound proteins by western blotting. Bub3 in

isolation did not bind MBP-Knl1^{MELT1}, in agreement with our previous data (Krenn et al.,

2014). The B3BD of Bub1 strongly enhanced binding of Bub3 to phosphorylated MBP-

Knl1^{MELT1} but not to unphosphorylated MBP-Knl1^{MELT1}, while the B3BD of BubR1 had

a negligible effect (Figure 2A). These results *in vitro* correlate with the ability of the

equivalent B3BD to support (or not) kinetochore recruitment in cells (Figure 1I-J).

Our previous structural and biochemical characterization of the Bub1^{B3BD}/Bub3/MELT^P

ternary complex of *S. cerevisiae* demonstrated that while Bub3 carries most of the crucial

(and evolutionarily conserved) residues involved in high-affinity binding to MELT^P, a

short segment of Bub1, the “loop”, contributes to the binding affinity (Primorac et al.,

2013). The “loop” region of Bub1 or BubR1 is between strands $\beta 1$ and $\beta 2$ (Figure 2B-D) and precedes the highly conserved core of the B3BD. The loop abuts the binding site for the MELT^P peptide and is therefore ideally positioned to modulate the binding affinity of Bub3 for MELT^P (Figure 2C-D).

Because the loops of Bub1 and BubR1 have quite divergent sequences (Figure 2B), we tested their role in modulating the binding affinity of Bub1²⁰⁹⁻²⁷⁰/Bub3 or BubR1³⁶²⁻⁴³¹/Bub3 for immobilized MBP-Knl1^{MELT1} (see Figure 2A). We swapped the loop regions of Bub1 and BubR1 as schematized in Figure 2E. Recombinant versions of the chimeric mutants Bub1^{209-270/BR1-loop} and BubR1^{362-431/B1-loop} were co-expressed with Bub3. Both the wild type and chimeric constructs interacted with apparently similar affinity with Bub3, excluding gross structural perturbations (Figure 2 Supplement 1). We then tested the ability of the recombinant constructs to interact with immobilized MBP-Knl1^{MELT1}. Bub1²⁰⁹⁻²⁷⁰ bound tightly and in an Mps1-phosphorylation-dependent manner to MBP-Knl1^{MELT1} (Figure 2F), while Bub1^{209-270/BR1-loop} bound weakly. Conversely, BubR1^{362-431/B1-loop} bound more strongly to phosphorylated MBP-Knl1^{MELT1} than did BubR1³⁶²⁻⁴³¹ (Figure 2F). These results demonstrate a crucial role of the loop region of Bub1 in the recognition of a phosphorylated MELT repeat.

IP experiments from stable cell lines expressing GFP fusions of the wild type or loop-swap mutants in the context of full length Bub1 or BubR1 recapitulated the results *in vitro* (Figure 2G-H). Loop swap mutants interacted with Bub3 as efficiently as wild type

counterparts, but the interactions that Bub3 mediates, most notably those with the Knl1 receptor and its associated partner Mis12, were strongly enhanced when the Bub1 loop region was grafted onto BubR1.

Behavior of the “loop swap” mutants in HeLa cells We then tested the localization behavior of these mutants. Kinetochores localization of GFP-Bub1^{B1-loop} was weaker than that of wild type Bub1 (Figure 3A-B), whereas kinetochores localization of GFP-BubR1^{B1-loop} was stronger than that of unmodified BubR1 (Figure 3C-D). Indeed, GFP-BubR1^{B1-loop} decorated kinetochores even after depletion of Bub1. Thus, when grafted onto BubR1, the Bub1 loop region is sufficient to confer upon BubR1 the ability to target kinetochores in a Bub1-independent fashion (Figure 3E-F). Although the experiments *in vitro* were carried out with a single MELT repeat, MELT1, they are likely to reflect the binding behavior of Bub1 and BubR1 to endogenous Knl1, which may contain up to 17 MELT repeats. Kinetochores localization of GFP-BubR1^{B1-loop} in cells depleted of Bub1 was inhibited by addition of Reversine, indicating a dependence on Mps1 and MELT^P sequences (Figure 3G-H and Figure 3 Supplement 1, panel A). Expression of BubR1^{B1-loop} did not overtly affect the kinetochores levels of endogenous Bub1 (Figure 3 Supplement 1, panel B), suggesting that the multiple MELT^P sequences of Knl1 are not saturated with endogenous Bub1 even in the strong checkpoint-activating conditions of our assay.

Next, we asked if GFP-BubR1^{B1-loop} was able to replace the SAC function of BubR1. In cells depleted of endogenous BubR1, wild type BubR1 restored SAC function to a high degree but GFP-BubR1^{B1-loop} failed to do so (Figure 3I). Comparison of immune-precipitates of GFP-BubR1 and of GFP-BubR1^{B1-loop} from nocodazole-treated mitotic cells showed much less of the latter associated with MCC and APC/C subunits (Figure 3J, quantified in Figure 3 Supplement 1, panel C). Similarly, immune-precipitation (IP) of the APC/C demonstrated association of GFP-BubR1, but not GFP-BubR1^{B1-loop}, with the APC/C (Figure 3K, quantified in Figure 3 Supplement 1, panel D). These results demonstrate that sequence divergence in the short loop region of Bub1 and BubR1 have strong functional consequences. In Bub1, the loop enhances the ability of Bub3 to recognize MELT^p sequences of Knl1. In BubR1, the precise role of the loop is unknown, but the results in Figure 3 suggest to us a specific role in MCC assembly or in the interaction with the APC/C, as discussed more thoroughly below.

A minimal BubR1-binding region of Bub1 The second question, how BubR1 is recruited to kinetochores, has three distinct facets. First, the segment of Bub1 required for kinetochore recruitment of BubR1 should be identified. Second, the segment of BubR1 required for its own kinetochore recruitment should be identified. Third, it should be established if Bub1 and BubR1 interact directly and if kinetochore proteins other than Bub1 play additional roles in BubR1 recruitment.

216 To investigate the role of Bub1 in BubR1 recruitment, we created GFP fusions of several
217 deletion mutants of Bub1 (Figure 1 Supplement 1C-D) and tested concomitantly their
218 kinetochore localization and BubR1 recruitment (Figure 4A). Bub1²⁰⁹⁻²⁷⁰, encompassing
219 the B3BD and localizing robustly to kinetochores, did not recruit BubR1 in cells depleted
220 of endogenous Bub1 (Figure 4A-B). A construct containing the tetratricopeptide repeats
221 (TPRs) and the B3BD of Bub1, Bub1¹⁻²⁸⁴, also targeted kinetochores but did not recruit
222 BubR1 (Figure 4A-B). On the contrary, a segment (Bub1²⁰⁹⁻⁴⁰⁹) consisting of the B3BD
223 and a ~140-residue C-terminal extension (CTE), targeted kinetochores and promoted
224 robust kinetochore localization of BubR1 (Figure 4A-B). Thus, Bub1 does not require
225 the CTE (residues 271-409) for its own kinetochore recruitment (the B3BD, residues
226 209-270, is sufficient), but requires it to recruit BubR1. A deletion mutant lacking the
227 CTE (Bub1^{Δ271-409}) targeted kinetochores efficiently but failed to recruit BubR1 (Figure
228 4C-D).

229 In IP experiments both in the presence and absence of endogenous Bub1, GFP-Bub1<sup>209-
230 409</sup> interacted with BubR1 at levels that were only modestly lower than those of full length
231 GFP-Bub1 (Figure 4E-F). Conversely, GFP-Bub1²⁰⁹⁻²⁷⁰ did not interact with BubR1, in
232 agreement with the inability of this construct to promote BubR1 localization. In this
233 context, it should be noted that the tetratricopeptide repeats (TPRs) near the N-
234 terminus of Bub1 and BubR1 (Figure 1A) had been initially identified as primary
235 determinants of kinetochore recruitment (Bolanos-Garcia et al., 2011; Kiyomitsu et al.,

236 2007), but later shown to be dispensable (Krenn et al., 2012; 2014), a result confirmed
237 here. In our IP experiments, however, we observe that Bub1 interacts with the outer
238 kinetochore more strongly when the TPRs are present, in agreement with our previous
239 studies (Krenn et al., 2012; 2014). The Bub1 TPR region interacts with a short sequence
240 motif of Knl1 named KI1 motif (Kiyomitsu et al., 2007; Krenn et al., 2012; 2014). This
241 interaction, whose precise significance is unclear, enhances the SAC response (Krenn et
242 al., 2014). Additional evidence of a modest additional role of the TPR in the interaction
243 of Bub1 and BubR1 with kinetochores is presented in Figure 4 Supplement 2 and Figure
244 4 Supplement 3.

245 Next, we asked if Bub1 binds directly to BubR1. Bub1¹⁻⁴⁰⁹ and BubR1¹⁻⁵⁷¹, both of which
246 target kinetochores (Elowe et al., 2010; Klebig et al., 2009; Malureanu et al., 2009; Taylor
247 et al., 1998; Vanoosthuyse et al., 2004), were individually co-expressed with Bub3 in
248 insect cells and purified to homogeneity. In size-exclusion chromatography (SEC)
249 experiments, in which the elution volume reflects macromolecular mass and shape,
250 BubR1¹⁻⁵⁷¹/Bub3 bound stoichiometrically to Bub1¹⁻⁴⁰⁹/Bub3 (Figure 4G), thus
251 demonstrating a direct interaction in the absence of other proteins. In these experiments
252 *in vitro*, BubR1¹⁻⁵⁷¹ did not require Bub3 to bind Bub1¹⁻⁴⁰⁹/Bub3 (Figure 4H), and
253 therefore in the following SEC experiments we used BubR1 and BubR1/Bub3
254 interchangeably (whereas Bub1 was poorly expressed and largely insoluble in insect cells
255 without Bub3). Although this result may suggest that Bub3 is not required for the

256 interaction of BubR1 with Bub1/Bub3, we show and discuss in the context of Figure 6
 257 that a functional B3BD is required for the interaction of BubR1 with Bub1 in living cells.
 258 In agreement with the ability of Bub1²⁰⁹⁻⁴⁰⁹ to recruit BubR1 to kinetochores, Bub1<sup>209-
 259 409</sup>/Bub3 formed a stoichiometric complex with BubR1¹⁻⁵⁷¹/Bub3 (Figure 4I) or BubR1<sup>1-
 260 571</sup> (Figure 4 Supplement 1, panel A), further showing that the Bub1 TPR region is
 261 dispensable. Neither the isolated B3BD of Bub1 (Bub1²⁰⁹⁻²⁷⁰/Bub3, Figure 4 Supplement
 262 1B) nor the isolated CTE (Bub1²⁷¹⁻⁴⁰⁹, Figure 4J) bound BubR1¹⁻⁵⁷¹/Bub3, indicating that
 263 both regions contribute to BubR1 binding *in vitro*. Additional SEC experiments
 264 supporting this conclusion are shown in Figure 4 Supplement 1, panels C-D.

265

266 ***A minimal Bub1-binding region of BubR1*** To identify a minimal kinetochore-
 267 targeting region of BubR1, we created GFP fusions of several deletion mutants of
 268 BubR1 (Figure 1 Supplement 1C-D) and tested their localization to kinetochores.
 269 BubR1³⁶²⁻⁵⁷¹, which contains the B3BD and a ~140-residue CTE, localized to
 270 kinetochores in a Bub1-dependent manner (Figure 5A-B). Shorter fragments of BubR1,
 271 including the isolated B3BD (BubR1³⁶²⁻⁴³¹, see also Figure 1J) and the isolated CTE
 272 (BubR1⁴³²⁻⁵⁷¹), did not localize to kinetochores (Figure 5B-C). In agreement with the
 273 kinetochore recruitment assay, SEC experiments showed binding of BubR1³⁶²⁻⁵⁷¹ but not
 274 of the isolated B3BD (BubR1³⁶²⁻⁴³¹/Bub3) or the isolated CTE (BubR1⁴³²⁻⁵⁷¹) to Bub1<sup>1-
 275 409</sup>/Bub3 (Figure 5D-F).

276

277 ***A pseudo-symmetric Bub1-BubR1 interaction*** Our results predict that BubR1³⁶²⁻⁵⁷¹
278 and Bub1²⁰⁹⁻⁴⁰⁹ ought to be sufficient for the Bub1/BubR1 interaction *in vitro*. Indeed,
279 BubR1³⁶²⁻⁵⁷¹ and Bub1²⁰⁹⁻⁴⁰⁹/Bub3 interacted stoichiometrically in SEC runs (Figure 6A).
280 A summary of the properties of the crucial Bub1 and BubR1 segments discussed in the
281 last two sections is presented in Figure 6B. An alignment of the interacting domains of
282 Bub1 and BubR1 (residues 209-409 and 362-571, respectively; the alignment was
283 obtained with programs Muscle [Edgar, 2004] and JPRED [Cole et al., 2008]) shows that
284 their sequences are structurally equivalent (Figure 6 Supplement 1A). Both start with the
285 B3BD, continue with a segment predicted to adopt a helical conformation and end with
286 a region predicted to lack defined secondary structure. We surmise that the ability of
287 modern-day Bub1 and BubR1 to form heterodimers using these structurally equivalent
288 (“pseudo-symmetric”) segments may reflect the ability of their ancestor to form
289 homodimers, similarly to what is observed in cohesins.

290

291 ***Functional dissection of kinetochore recruitment of BubR1*** Deletion of residues
292 432-484 of BubR1 (GFP-BubR1^{Δ432-484}) in the predicted helical region impaired
293 kinetochore localization of BubR1 (Figure 6C-D). Additionally, mutations in the B3BD
294 of BubR1 (E409K+E413K) known to impair Bub3 binding (Larsen et al., 2007; Taylor et
295 al., 1998) prevented kinetochore localization of full length BubR1 (Figure 6E-F) and of

296 BubR1³⁶²⁻⁵⁷¹ (Figure 6 Supplement 1, panels B-C). Thus, Bub3 binding is necessary for
297 efficient kinetochore localization of BubR1 even if it may appear to be dispensable for
298 the interaction *in vitro* (Figure 4H). We note that in those SEC binding experiments *in*
299 *vitro* in which we used isolated BubR1 rather than BubR1/Bub3, Bub3 might have
300 exchanged from the Bub1/Bub3 complex to reconstitute BubR1/Bub3. Alternatively,
301 the relatively high protein concentrations in the SEC experiments (5-15 μ M) may
302 effectively compensate for reduced binding affinity when BubR1 is devoid of Bub3.

303 Regardless of the precise explanation, BubR1 clearly requires Bub3 for efficient
304 kinetochore localization. This requirement may reflect a direct contribution to the
305 interaction with Bub1 or alternatively a residual ability of BubR1/Bub3 to bind
306 phosphorylated motifs on Knl1 or other kinetochore proteins. To try distinguishing
307 between these possibilities, we targeted a Lac repressor (LacI) fusion of Bub1 to an
308 ectopic Lac operator (LacO) site on the chromosome distinct from centromeres. LacI-
309 Bub1 recruited BubR1 to the ectopic site (Figure 6G-H, quantified in Figure 6
310 Supplement 1D), thus suggesting that kinetochores are not required for the
311 Bub1/BubR1 interaction, in agreement with a previous study in *S. pombe* (Rischitor et al.,
312 2006). This result suggests that Bub1/Bub3 is sufficient for recruitment of BubR1/Bub3,
313 and that the role of Bub3 in recruitment of BubR1 might be direct and not through
314 Knl1. Mutation of the Bub3-binding site of the LacI-Bub1 fusion (Bub1^{E252K}) prevented
315 BubR1 recruitment, suggesting that Bub3 is required for a robust interaction between

316 Bub1 and BubR1 on both sides of the complex (Figure 6G-H).

317 BubR1 is important for the SAC and for establishing bi-orientation. We therefore asked

318 if perturbing its kinetochore localization impaired these processes. HeLa cells depleted of

319 endogenous BubR1 failed to arrest in mitosis in the presence of nocodazole (Figure 7A).

320 SAC proficiency was re-established upon expression of GFP-BubR1 but not GFP-

321 BubR1^{E409K+E413K}. GFP-BubR1^{Δ432-484}, on the other hand, restored a robust SAC response.

322 IP experiments indicated that both GFP-BubR1^{E409K+E413K} and GFP-BubR1^{Δ432-484} were

323 unable to interact with Bub1 or Knl1, as expected based on their localization behavior.

324 However, GFP-BubR1^{E409K+E413K} was also significantly impaired in its ability to interact

325 with two additional MCC subunits (Mad2 and Cdc20), and was even more dramatically

326 impaired in its ability to interact with the APC/C. Conversely, GFP-BubR1^{Δ432-484}

327 interacted with the MCC subunits (including Bub3, as expected) and with the APC/C at

328 levels that were comparable to those of the wild type GFP-BubR1 control (Figure 7B).

329 Thus, two distinct mutants of BubR1 both impaired in kinetochore localization have

330 uncorrelated behaviors with regard to SAC proficiency. On the other hand, because

331 GFP-BubR1^{E409K+E413K} does not bind Bub3, while GFP-BubR1^{Δ432-484} does (Figure 7B,

332 quantified in Figure 7C), it appears that at least in human cells BubR1 needs to bind

333 Bub3 to become incorporated into the MCC.

334 In addition to playing a role in the SAC, BubR1 is important for establishing bi-

335 orientation in HeLa cells, and this role requires its kinetochore recruitment (Johnson et

al., 2004; Kruse et al., 2013; Lampson and Kapoor, 2005; Meraldi and Sorger, 2005; Suijkerbuijk et al., 2012b; Xu et al., 2013). Both GFP-BubR1^{E409K+E413K} and GFP-BubR1^{Δ432-484}, neither of which localizes to kinetochores, failed to complement the deficits in promoting the formation of stable kinetochore-microtubule attachments observed in cells depleted of endogenous BubR1 (Figure 7D). The role of BubR1 in kinetochore-microtubule attachment has been attributed to its interaction with the B56 regulatory subunit of a complex of protein phosphatase 2A (PP2A^{B56}) (Kruse et al., 2013; Suijkerbuijk et al., 2012b; Xu et al., 2013; Espert et al., 2014; Nijenhuis et al., 2014). Recently, this function of BubR1 has been further implicated in SAC silencing (Espert et al., 2014; Nijenhuis, et al., 2014). We asked if the defect of the BubR1^{Δ432-484} mutant in supporting kinetochore-microtubule attachment correlated with a defective interaction with PP2A^{B56}. Indeed, the levels of the B56 regulatory subunit in IPs of the GFP-BubR1^{Δ432-484} mutant were much lower than those of the wild type protein (Figure 7E).

Discussion

New genes are frequently created by duplication (Conant and Wolfe, 2008). After duplication, the paralogs (i.e. the genes generated by the duplication event) may diverge and sub-functionalize, thus allowing specialization in a subset of the functions originally provided by the singleton (the single ancestor gene before duplication) (Conant and Wolfe, 2008). The resolution of adaptive conflicts between different functions of the

356 singleton has been identified as a beneficial consequence of gene duplication (Hittinger
357 and Carroll, 2007). Detailed molecular illustrations of this process, however, are rare.

358 Our analysis of the mechanism of recruitment of Bub1 and BubR1 illustrates how the
359 duplication of an ancestor gene and subsequent divergence was exploited during
360 evolution to create two gene products with highly diversified and efficient functions,
361 including monitoring checkpoint status through stable recruitment to unattached
362 kinetochores (Bub1), effecting APC/C inhibition through incorporation into the MCC
363 (BubR1), stabilization of microtubule attachment (Bub1 and BubR1, possibly through
364 different mechanisms), and SAC silencing (BubR1). The occurrence of nine distinct
365 duplications of the Bub1 and BubR1 ancestor (Suijkerbuijk et al., 2012a) likely reflects an
366 extreme evolutionary pressure to separate functions that were originally condensed in a
367 single gene. Investigating to what extent sub-functionalization after each of the nine
368 distinct duplication events of the Bub1 and BubR1 ancestor followed similar or divergent
369 paths will be an interesting direction for future studies.

370 Previously, the loss of kinase activity specifically in BubR1 but not Bub1 was identified as
371 a manifestation of the divergence of these proteins (Vleugel et al., 2012; Suijkerbuijk et
372 al., 2012b). Here, we have considerably extended our understanding of this divergence by
373 showing that the loop motifs in the B3BDs of Bub1 and BubR1 modulate the interaction
374 of Bub3 with MELT^P. A suboptimal loop region for MELT^P binding in BubR1 makes it
375 depend on an alternative mechanism for kinetochore localization. This alternative is the

376 direct interaction with Bub1, extensively characterized in Figures 4-6. By swapping loop
377 motifs, we created a gain-of-function mutant of BubR1 that can bind kinetochores in the
378 absence of Bub1, and a loss-of-function mutant Bub1 severely impaired in autonomous
379 kinetochore binding. The failure of the BubR1 gain-of-function mutant to complement
380 the depletion of wild type BubR1 strongly suggests that the evolutionary divergence of
381 Bub1 and BubR1, with its specific effects on kinetochore recruitment, is functionally
382 relevant.

383 The mechanism of BubR1 localization depends on a direct, pseudo-symmetric hetero-
384 dimerization interaction with Bub1 (Figure 8A). It involves equivalent segments of Bub1
385 and BubR1 comprising their B3BD/GLEBS motif and a CTE whose first part is
386 predicted to be helical. The interaction of Bub1 and BubR1 requires that each have a
387 bound Bub3. Thus, Bub3 has at least three distinct functions: 1) it recruits Bub1 to
388 MELT^p motifs of Knl1; 2) it contributes to the dimerization of Bub1 with BubR1
389 required for kinetochore recruitment of the latter; and 3) in complex with BubR1, it has
390 an additional hitherto unknown function in the SAC. This function was exposed by the
391 behavior of the BubR1^{E409K+E413K} mutant. The SAC defect observed with this mutant is
392 unlikely to be a consequence of impaired kinetochore localization, because another
393 kinetochore-localization impaired mutant, BubR1^{Δ432-484}, was checkpoint proficient. We
394 surmise that BubR1-bound Bub3 is involved in an unknown aspect of the SAC
395 mechanism downstream of kinetochores, possibly having to do with MCC establishment

396 or APC/C binding, as recent proposed (Han et al., 2014). In analogy with the role of the
397 Bub1 loop motif in modulating the function of Bub3 as a MELT^P receptor, we speculate
398 that the BubR1 loop motif influences the specificity of BubR1-bound Bub3 for
399 additional SAC-relevant targets. The fact that the “loop swap” BubR1 mutant is unable
400 to sustain the SAC provides evidence for this hypothesis. The properties of the loop
401 region in the recently discovered protein BuGZ, which contains a B3BD/GLEBS motif
402 that interacts with Bub3, are also of interest (Jiang et al., 2014; Toledo et al., 2014).

403 Recruitment of PP2A^{B56} by BubR1 has been recently implicated in SAC silencing through
404 a mechanism ultimately impinging on dephosphorylation of the MELT^P motifs (Espert
405 et al., 2014; Nijenhuis et al., 2014). The apparent checkpoint proficiency of BubR1^{Δ432-484}
406 may indicate that BubR1 localization to kinetochores is not essential for checkpoint
407 function, as it implies that substantial amounts of MCC can be generated even when
408 BubR1/Bub3 cannot be recruited to kinetochores. However, we note that this mutant
409 interacts only weakly with PP2A^{B56} and might therefore carry an additional checkpoint-
410 silencing defect obscuring an underlying SAC defect. Furthermore, we cannot exclude
411 that residues in the deleted segments (432-484) of BubR1 are normally involved in an
412 intra-molecular control mechanism that couples the activation of wild-type BubR1 to
413 kinetochore recruitment.

414 Whether or not BubR1 kinetochore recruitment is important for SAC function, it is
415 clearly essential for kinetochore-microtubule attachment and bi-orientation. Previously, it

416 has been shown that BubR1 promotes bi-orientation through recruitment of PP2A^{B56}
 417 (Kruse et al., 2013; Suijkerbuijk et al., 2012b; Xu et al., 2013), which counteracts Aurora
 418 B activity and thus stabilizes kinetochore-microtubule attachments (Foley et al., 2011;
 419 Lampson and Kapoor, 2005). Our results demonstrate that BubR1^{Δ432-484}, which cannot
 420 interact with Bub1 and localize to kinetochores, has a strong defect in kinetochore-
 421 microtubule attachment that correlates with a defective interaction with PP2A^{B56}.
 422 Dissecting the requirement for kinetochore recruitment of the SAC subunits is
 423 instrumental for distinguishing their roles in the SAC from their roles in chromosome bi-
 424 orientation (Brady and Hardwick, 2000; De Antoni et al., 2005; London and Biggins,
 425 2014; London et al., 2012; Nijenhuis et al., 2013; Shepperd et al., 2012; Yamagishi et al.,
 426 2012; Moyle et al., 2014). By describing the mechanism of BubR1 recruitment and the
 427 role of the loop motif of Bub1 and BubR1 in modulating the affinity for kinetochores,
 428 this study fills an important gap. We and others have previously shown that two
 429 conformers of Mad2, O-Mad2 and C-Mad2, form an asymmetric conformational dimer
 430 (De Antoni et al., 2005; Luo et al., 2004). In this reaction, Mad1 acts as a stable
 431 placeholder for C-Mad2 (De Antoni et al., 2005). Once at kinetochores, the Mad1/C-
 432 Mad2 complex recruits a high-turnover cytosolic form of O-Mad2, and converts it into
 433 the active C-Mad2 form, which targets Cdc20, thus overcoming a rate-limiting step
 434 towards the formation of MCC (De Antoni et al., 2005; Mapelli et al., 2007; Simonetta et
 435 al., 2009). This scheme, summarized in Figure 8B, identifies Mad1/Mad2 as a “template”

for the establishment of the Cdc20/C-Mad2 complex, a structural “copy” of the Mad1/Mad2 complex (De Antoni et al., 2005; Musacchio and Salmon, 2007).

Even if directed primarily towards a different function (SAC signaling rather than chromosome bi-orientation), we note that this pattern is remarkably similar to that emerging from the mechanism of BubR1 recruitment by Bub1, in which a stable Bub1/Bub3 complex at kinetochores recruits a rapidly cycling BubR1/Bub3 complex. The MCC, made of Cdc20/C-Mad2 and BubR1/Bub3, can be interpreted as a “copy” of kinetochore-bound “templates” made of Mad1/C-Mad2 and Bub1/Bub3 complexes. Whether such templates engage in a complex at kinetochores is unclear but plausible. Even if we did not identify Mad1 in our mass spectrometry analysis of Bub1, we recently identified both Mad1 and Bub1 in precipitates of the N-terminal segment of Knl1 (Krenn et al., 2014). Furthermore, Mad1 and Bub1 have been shown to interact directly in *S. cerevisiae* and *C. elegans* (Brady and Hardwick, 2000; London et al., 2012; Moyle et al., 2014). Our future studies will aim to investigate the significance of the copy-template molecular relationship for SAC signaling and chromosome bi-orientation.

Methods

Mammalian plasmids Plasmids were derived from the pCDNA5/FRT/TO-EGFP-IRES, a previously modified version (Krenn et al., 2012) of the pCDNA5/FRT/TO vector (Invitrogen). To create N-terminally-tagged EGFP Bub1 and BubR1 truncation constructs, Bub1 and BubR1 sequences were obtained by PCR amplification from the previously generated pCDNA5/FRT/TO-EGFP-Bub1-IRES and pCDNA5/FRT/TO-

EGFP-BubR1-IRES vector, respectively (Krenn et al., 2012) and subcloned in frame with the GFP-tag. Mutations and deletions within the Bub1 and BubR1 constructs were generated by standard site-directed mutagenesis or by a mutagenesis protocol (Liu and Naismith, 2008). All Bub1 constructs were RNAi resistant (Kiyomitsu et al., 2007). BubR1-expressing constructs were made siRNA-resistant by changing the sequence targeted by the RNAi oligos to 'AACGTGCCTTCGAGTACGAGA'. pCDNA5/FRT/TO-based plasmids were used for generation of stable cell lines, as well as for transient transfection. All plasmids were verified by sequencing.

Cell culture and transfection HeLa cells were grown in DMEM (PAN Biotech) supplemented with 10 % FBS (Clontech), penicillin and streptomycin (GIBCO) and 2 mM L-glutamine (PAN Biotech). For all plasmid transfections of HeLa cells XtremeGENE transfection agent (Roche) was used at a 3:1 ratio with plasmid DNA. Flp-In T-REx HeLa cells used to generate stable doxycycline-inducible cell lines were a gift from S.S. Taylor (University of Manchester, Manchester, England, UK). Flp-In T-REx host cell lines were maintained in DMEM with 10 % tetracycline-free FBS (Clontech) supplemented with 50 µg/ml Zeocin (Invitrogen). Flp-In T-REx HeLa expression cell lines were generated as previously described (Krenn et al., 2012). Gene expression was induced by addition of 0.2 -0.5 µg/ml doxycycline (Sigma) for 24 hours. siBUB1 (Dharmacon; 5'-GGUUGCCAACACAAGUUCU-3') or siBUBR1 (Dharmacon; 5'-CGGGCAUUUGAAUAUGAAA-3') duplexes were transfected with Lipofectamine 2000 (Invitrogen) at 50 nM for 24 hours.

For experiments in HeLa cells, cells were synchronized with a double thymidine arrest 5 h after transfection with siRNA duplexes. In brief, after washing the cells with PBS they were treated with thymidine for 16 hours and then released into fresh medium. 3 hours after the release, 50 nM siRNA duplexes were transfected again. 5 hours after transfection, cells were treated with thymidine for 16 hours and afterwards released in fresh medium. Unless differently specified, nocodazole (Sigma-Aldrich) was used at 3.3 µM. MG132 (used at 5-10 µM) was obtained from Calbiochem, thymidine (2 mM) was purchased from Sigma-Aldrich. Reversine (Calbiochem) was used at 0.5 µM.

Immunoprecipitation and immunoblotting To generate mitotic populations for immunoprecipitation experiments, cells were treated with 330 nM nocodazole for 16 h. Mitotic cells were then harvested by shake off and lysed in lysis buffer [150 mM KCl, 75 mM Hepes, pH 7.5, 1.5 mM EGTA, 1.5 mM MgCl₂, 10 % glycerol, and 0.075 % NP-

40 supplemented with protease inhibitor cocktail (Serva) and PhosSTOP phosphatase inhibitors (Roche)]. Extracts were precleared using a mixture of protein A-Sepharose (CL-4B; GE Healthcare) and protein G-Sepharose (rec-Protein G-Sepharose 4B; Invitrogen) for 1 hour at 4 °C. Subsequently, extracts were incubated with GFP-Traps (ChromoTek; 3 µl/mg of extract) for 3 hours at 4 °C. Immunoprecipitates were washed with lysis buffer and resuspended in sample buffer, boiled and analyzed by SDS-PAGE and Western blotting using 4-12 % gradient gels (NuPAGE® Bis-Tris Gels, Life technologies). For Cdc27 IPs cells were synchronized by addition of the CDK1-inhibitor RO3306 (Calbiochem) for 15 hours and subsequently released into 330 nM nocodazole for 2-3 hours before harvesting by shake off. Cells were lysed in lysis buffer (described above) and extracts were precleared with protein G-Sepharose for 1 hour at 4 °C. Afterwards, extracts were incubated with 1.5 µg/mg of the Cdc27 primary antibody (mouse monoclonal, BD) for 2 hours at 4 °C. Subsequently, protein G-Sepharose was added for 4 hours at 4 °C. Immunoprecipitates were washed and analyzed as described above. The following antibodies were used: anti-GFP (in house made rabbit polyclonal antibody; 1:1000-3000), anti-Mis12 (in house made mouse monoclonal antibody; clone QA21-74-4-3; 1:1000), anti-Knl1-N (in house made rabbit polyclonal SI0787 antibody; 1:1000), anti-Bub1 (rabbit polyclonal; Abcam; 1:5000), anti-BubR1 (mouse monoclonal; BD; 1:1000), anti-Bub3 (mouse monoclonal; BD; 1:1000), anti-Tubulin (mouse monoclonal; Sigma; 1:8000), anti-Apc7 (in house made rabbit polyclonal antibody SI0651, 1:500), anti-Cdc20 (mouse monoclonal, Santa Cruz, 1:500), anti-Mad2 (in house made mouse monoclonal antibody, clone AS55-A12, 1:500), anti-Cdc27 (mouse monoclonal, BD; 1:1000-3000), anti-PP2A^{B56α} (rabbit polyclonal; Bethyl; 1:1000). Secondary antibodies were anti-mouse (Amersham) and anti-rabbit (Amersham) affinity-purified with horseradish peroxidase conjugate (working dilution 1:10000) or Protein G with horseradish peroxidase conjugate (Life technologies) (working dilution 1:6000). After incubation with ECL Western blotting system (GE Healthcare), images were acquired with ChemiBIS 3.2 (DNR Bio-Imaging Systems) in 16-bit TIFF format. Levels of images were adjusted using Image J software and then cropped and converted to 8-bit. Unmodified 16-bit TIFF images were used for quantification with Image J software. Measurements were graphed with Excel (Microsoft) and GraphPad Prism version 6.0 for Mac OS X (GraphPad Software, San Diego California USA).

Live cell imaging Cells were plated on a 24-well µ-Plate (Ibidi®). Drugs were diluted in

CO₂ Independent Medium (Gibco®) and added to the cells 1 hour before filming. Cells were imaged every 20 to 30 min in a heated chamber (37 °C) on a 3i Marianas™ system (Intelligent Imaging Innovations Inc.) equipped with Axio Observer Z1 microscope (Zeiss), Plan-Apochromat 40x/1.4NA oil objective, M27 with DIC III Prism (Zeiss), Orca Flash 4.0 sCMOS Camera (Hamamatsu) and controlled by Slidebook Software 5.5 (Intelligent Imaging Innovations Inc). For cells expressing the GFP-BubR1 proteins, only cells in which kinetochores were visible were considered for the analysis.

Immunofluorescence HeLa cells and Flp-In T-REx HeLa cells were grown on coverslips precoated with poly-D-Lysine (Millipore, 15 µg/ml) and poly-L-Lysine (Sigma), respectively. For the experiments with Hela cells, cells were synchronized with a double thymidine block and after release from that arrested in prometaphase by the addition of 330 nM nocodazole for 3 hours. For all other experiments, asynchronously growing cells were arrested in prometaphase by the addition of nocodazole for 3-4 hours and fixed using 4 % paraformaldehyde. Cells were stained for Bub1 (mouse, ab54893, 1:400), BubR1 (rabbit, Bethyl A300-386A, 1:1000), CREST/anti-centromere antibodies (Antibodies, Inc., 1:100), diluted in 2 % BSA-PBS for 1.5 hours. Goat anti-human and chicken anti-rabbit Alexa Fluor 647 (Invitrogen), goat anti-rabbit and anti-mouse RRX and donkey anti-human Alexa Fluor 405 (Jackson ImmunoResearch Laboratories, Inc.) were used as secondary antibodies. DNA was stained with 0.5 µg/ml DAPI (Serva) and coverslips were mounted with Mowiol mounting media (Calbiochem). Cells were imaged at room temperature using a spinning disk confocal device on the 3i Marianas™ system equipped with an Axio Observer Z1 microscope (Zeiss), a CSU-X1 confocal scanner unit (Yokogawa Electric Corporation), Plan-Apochromat 63x or 100x/1.4NA Oil Objectives (Zeiss) and Orca Flash 4.0 sCMOS Camera (Hamamatsu). Images were acquired as z-sections at 0.27 µm. Images were converted into maximal intensity projections, exported and converted into 8-bit. Quantification of kinetochore signals was performed on unmodified 16-bit z-series images using Imaris 7.3.4 32-bit software (Bitplane). After background subtraction, all signals were normalized to CREST. At least 138 kinetochores were analyzed per condition. Measurements were exported in Excel (Microsoft) and graphed with GraphPad Prism 6.0 (GraphPad Software, San Diego California USA).

For analysis of cold-stable microtubules, cells that were synchronized with a single Thymidine arrest, released for 6.5 hours and kept for 4 hours in 5 µM MG132, were

incubated for 5 min on ice in medium with 10 mM HEPES pH 7.5 and then directly fixed in 4 % PFA. Cells were stained for Tubulin (mouse, Sigma T9026, 1:5000) and CREST. DNA was labeled with DAPI. CREST staining was used to identify kinetochores in image z-stacks to count kinetochores attached to cold-stable microtubules. Each kinetochore was classified as “attached” or “not attached” depending on whether a microtubule fiber ended at the kinetochore. An average of 120 kinetochores was counted per cell and seven cells were analyzed for each condition.

Expression and purification of MBP-Knl1¹³⁸⁻¹⁶⁸-H6 MBP-Knl1¹³⁸⁻¹⁶⁸-H6 and MBP-Knl1¹³⁸⁻¹⁶⁸-H6 constructs (MELT1) were obtained by sub-cloning into a pGEX vector backbone in which the coding sequence for GST was replaced with that for MBP. Expression was carried out in BL21 RIL strain at 25°C and by using 1 mM IPTG for 2.5 hours to induce expression. Cell pellets were re-suspended in 3 pellet volumes of 50 mM HEPES-NaOH pH 7.5, 250 mM KCl, 2 mM DTE, 10% glycerol, protease inhibitor mix (Serva). Cells were lysed by sonication, and the lysates were centrifuged at 100000 x g for 1 hour at 4°C. Recombinant products were isolated from the lysate by using the HisTrap (GE Healthcare) column, followed by buffer exchange using a desalting column (GE Healthcare). Purified proteins were concentrated to about 3 mg/ml and frozen in liquid nitrogen.

Expression and purification of H6-BubR1³⁶²⁻⁴³¹/Bub3 and H6-Bub1²⁰⁹⁻²⁷⁰/Bub3 constructs GST-BubR1³⁶²⁻⁴³¹/Bub3 and GST-Bub1²⁰⁹⁻²⁷⁰/Bub3 constructs were obtained by sub-cloning the coding sequences for Bub3 and for the indicated segments of Bub1 into pFLMultiBac vector (Trowitzsch et al., 2010). Expression was carried out by infection of Tna38 insect cells (Hashimoto et al., 2012) for 72 hours at 27°C. Viruses of the constructs were generated as described (Trowitzsch et al., 2010). Insect cells were harvested by centrifugation at 1500 rpm for 30 min in a Sorvall RC 3BP+ (Thermo Scientific) centrifuge with Rotor H6000A, and the pellets were frozen in liquid nitrogen and stored at -80°C. 1 g of cell pellet was re-suspended in 10 ml lysis buffer (50 mM Tris-HCl pH 8.0 or 8.5, 150 mM KCl, 2 mM DTE, DNase, PMSF, protease inhibitors (Serva)). Cells were lysed by sonication and the lysate centrifuged at 100000 g for 1 hour at 4°C. The supernatant was filtered through Nalgene bottle-top filter. 1.5 ml of GSH bead slurry (GE Healthcare) was added to 50 ml of cleared lysate. After 1 hour at 4°C on a rotating wheel the beads were recovered by centrifugation and washed with lysis buffer. Bead-bound complexes in 50 ml of lysis buffer were retrieved from the GSH beads by

addition of GSH-Prescission protease (produced in house) for 14 hours at 4°C. Eluates were concentrated using Amicon concentrators (3 kDa cutoff), diluted with 20 mM Tris-HCl, 2 mM DTE to a final KCl concentration of 50 mM, and further purified using 1 ml HiTrap QFF column (GE Healthcare). Peak fractions were collected and concentrated down to a volume of 2 ml and further purified by size exclusion chromatography using the S75 16/60 column (GE Healthcare). Peak fractions were collected, concentrated to about 3 mg/ml, frozen in small aliquots in liquid nitrogen and stored at -80°C. Sequences of loop swap constructs were as follows:

Bub1²⁰⁹⁻²⁷⁰

RRVITISKSEYSVHSSLASKVDVEQVVMYCKEKLIRGESEFSFEELRAQKYNQR
RKHEQWVN

Bub1²⁰⁹⁻²⁷⁰-BubR1 loop

RRVITTRKPGKEEGDPLSKVDVEQVVMYCKEKLIRGESEFSFEELRAQKYNQR
RKHEQWVN

BubR1³⁶²⁻⁴³¹

INHILSTRKPGKEEGDPLQVRVQSHQQASEEKKEKMMYCKEKIYAGVGEFSFE
EIRAEVFRKKLKEQREAE

BubR1³⁶²⁻⁴³¹-Bub1 loop

INHILSISKSEYSVHSSLAQVRVQSHQQASEEKKEKMMYCKEKIYAGVGEFSFEE
IRAEVFRKKLKEQREAE

Expression and purification of H6-BubR1¹⁻⁵⁷¹, H6-BubR1¹⁻⁵⁷¹/Bub3, H6-BubR1²²²⁻⁵⁷¹/Bub3, H6-Bub1¹⁻⁴⁰⁹/Bub3, H6-Bub1¹⁻⁴⁰⁹/Bub3-TRX and H6-Bub1¹⁻²⁸⁰/Bub3

Sequences coding for H6-BubR1, H6-Bub1 and untagged Bub3 constructs were sub-cloned into pFLMultiBac vectors and baculoviruses were generated. Baculovirus expressing Bub3-TRX was generated by the Dortmund Protein Facility (DPF) using the pOPIN vector system {Berrow:2007cy}. Bub1/Bub3 and BubR1/Bub3 complexes were generated by co-infection and co-expression at 27 °C for 72 hours. Insect cells were harvested by centrifugation at 1500 rpm for 30 minutes in a Sorvall RC 3BP+ (Thermo Scientific) centrifuge with Rotor H6000A, the pellets were frozen in liquid nitrogen and stored at -80 °C. 1 g of cell pellet was re-suspended in 10 ml Lysis buffer [50 mM HEPES-KOH pH 7.5, 150 mM KCl, 15 mM imidazole, 2 mM DTE, 0.05% Tween20,

PMSF, protease inhibitors (Serva)]. Cells were lysed by sonication and centrifuged at 100000 g for 1 hour at 4°C. The supernatant was filtered through Nalgene bottle-top filter. The complexes were isolated from the cleared lysate on a 5 ml HisTrap (GE Healthcare) column. Peak fractions were pooled concentrated using Amicon concentrators and further purified in GF buffer (50 mM Hepes-KOH pH 7.5, 150 mM KCl, 2 mM DTE, 0.05% Tween20) by size exclusion chromatography using S200 16/60 column (GE Healthcare). Peak fractions were pooled, concentrated to typically 3 to 5 mg/ml and frozen in liquid nitrogen.

Expression and purification of H6-Bub1²⁷¹⁻⁴⁰⁹-MBP, H6-Bub1²⁰⁹⁻⁴⁰⁹-MBP/Bub3, H6-TRX-BubR1³⁶²⁻⁵⁷¹, H6-TRX-BubR1⁴³²⁻⁵⁷¹ Sequences encoding H6-TRX-BubR1, H6-Bub1-MBP and untagged Bub3 constructs were sub-cloned into pFLMultiBac vectors and baculoviruses were generated. All constructs, apart from H6-Bub1²⁰⁹⁻⁴⁰⁹-MBP, which was co-expressed with untagged Bub3, were expressed individually in insect cells at 27 °C for 72 hours. Insect cells were harvested by centrifugation at 1500 rpm for 30 min in a Sorvall RC 3BP+ (Thermo Scientific) centrifuge with Rotor H6000A, the pellets were frozen in liquid nitrogen and stored at -80 °C. 1 g of cell pellets were re-suspended in 10 ml Lysis buffer [50 mM Tris-HCl pH 7.5, 150 mM KCl, 0.5 mM β-mercaptoethanol, 0.05% NP40, PMSF, protease inhibitors (Serva)]. Cells were lysed by sonication and centrifuged at 100000g for 1 hour at 4 °C. The supernatant was filtered through Nalgene bottle-top filter. The complexes were isolated from the cleared lysate on a 5 ml TALON column (Clontech). Peak fractions were pooled, concentrated and further purified in GF buffer (50 mM Tris-HCl pH 8.0, 150 mM KCl, 2 mM TCEP) by size exclusion chromatography on a S75 16/60 or S200 16/60 column. Peak fractions were pooled, concentrated to typically 3 to 5 mg/ml, frozen in small aliquots in liquid nitrogen and stored at -80 °C.

Size exclusion chromatography mobility shift assay Proteins tested for interactions were diluted to 15 μM in 150 μl reactions in GF buffer (50 mM Tris-HCl pH 8, 150 mM KCl, 1.5 mM TCEP, 0.05% Tween20) and incubated at 20-22 °C for 1 hour on a rotating wheel. 100 μl of the resulting incubation were analyzed by size exclusion chromatography on a Superose6 10/300 column at a flow rate of 0.4 ml/min and collected in 300 μl fractions. Eluates were analyzed by SDS PAGE and Coomassie staining.

In vitro binding assays 5 μg of MBP-Knl1^{MELT1}-H6 protein were phosphorylated with Mps1 kinase (ITK, Life technologies) in a 35 μl reaction in 12.5 mM Tris-HCl pH 7.5, 35 mM

KCl, 10 mM MgCl₂, 0.5 mM EGTA, 0.005 % Triton X-100, 2 mM TCEP, 0.5 μM Okadaic acid, at 30 °C for 1 hour, 1200 rpm. BSA was added to a final concentration of 2 mg/ml, and the reaction was incubated with 20 μl Amilose resin (New England Biolabs) for 1 hour at room temperature. The beads were washed with 50 mM HEPES-NaOH pH 7.5, 150 mM KCl, 0.05 % Tween-20, 2mM DTE. 20 μl Knl1-bound resin was then incubated in 50 μl of a 400 nM solution of prey proteins (e.g. H6-BubR1³⁶²⁻⁴³¹/Bub3 or H6-Bub1²⁰⁹⁻²⁷⁰/Bub3 or loop swap constructs) in 50 mM HEPES-NaOH pH 7.5, 50 mM KCl, 0.05 % Tween-20, 2 mM DTE, 10 % glycerol, 4 mg/ml BSA, for 1 hour at room temperature. Unbound proteins were removed with 50 mM HEPES-NaOH pH 7.5, 150 mM KCl, 0.05% Tween-20, 2 mM DTE. 20 μl of the resin were boiled in 70 μl of sample buffer, separated on 10 % gel and blotted with anti-Bub3 (mouse monoclonal, BD, 1:1000) or anti-MBP (mouse monoclonal, New England Biolabs, 1:10000) antibodies.

Mass spectrometry Cells were adapted to Lys-0/Arg-0 (Light) medium or Lys-8/Arg-10 (Heavy) medium for two weeks. Cells were synchronized in mitosis by a 24-hour thymidine block, followed by a 14 hour treatment with nocodazole. After harvesting the mitotic population, cells were split in the presence of either 500 nM Reversine for 30 min or with DMSO as a control. LAP-BUB1 or LAP-KNL1 expression was induced for 24 hours using doxycycline and cells were harvested and mixed, followed by immunoprecipitation and mass spectrometry. Cells were lysed at 4°C in hypertonic lysis buffer (500 mM NaCl, 50 mM Tris-HCl (pH 7.6), 0.1% sodium deoxycholate, 1 mM DTT) including phosphatase inhibitors (1 mM sodium orthovanadate, 5 mM sodium fluoride, 1 mM β-glycerophosphate), sonicated, and LAP-tagged proteins were coupled to GFP-trap (ChromoTek) for 1 hour at 4°C. Purifications were washed three times with high-salt (2 M NaCl, 50 mM Tris-HCl (pH 7.6), 0.1 % sodium deoxycholate, 1 mM DTT) and low-salt wash buffers (50 mM NaCl, 50 mM Tris-HCl (pH 7.6), 1 mM DTT) and subsequently eluted in 2 M Urea, 50 mM Tris-HCL (pH 7.6), 5 mM IAA. Samples were loaded on a C18 reverse phase column and ran on a nano-LC system coupled to a mass spectrometer (LTQ-Orbitrap Velos; Thermo Fisher Scientific) via a nanoscale LC interface (Proxeon Biosystems, now Thermo Fisher Scientific), as described in (Suijkerbuijk et al., 2012).

LacO experiments. U2OS LacO cells (a gift from S. Janicki) were grown in DMEM supplemented with 8 % FBS (Clontech), hygromycin (200 μg/ml), pen/strep (50 μg/ml)

and L-glutamine (2 mM). Cells were transfected with the indicated constructs for 48 hours using Fugene HD according to the manufacturer's protocol. Asynchronously growing cells were arrested in prometaphase by the addition of nocodazole (830 nM) for 2-3 hours. Cells plated on 12-mm coverslips were fixed (with 3.7 % paraformaldehyde, 0.1 % Triton X-100, 100 mM Pipes, pH 6.8, 1 mM MgCl₂, and 5 mM EGTA) for 5-10 min. Coverslips were washed with PBS and blocked with 3% BSA in PBS for 1 hour, incubated with primary antibodies (GFP-booster [Chromotek], rabbit-anti-BUBR1 [Bethyl] and CREST/anti-centromere antibodies [Cortex Biochem, Inc.]) for 16 hour at 4°C, washed with PBS containing 0.1 % Triton X-100, and incubated with secondary antibodies (goat-anti-rabbit Alexa Fluor 568 and goat anti-human Alexa Fluor 647) for an additional hour at room temperature. Coverslips were then washed, incubated with DAPI for 2 min, and mounted using antifade (ProLong; Molecular Probes). All images were acquired on a deconvolution system (DeltaVision RT; Applied Precision) with a 100×/1.40 NA U Plan S Apochromat objective (Olympus) using softWoRx software (Applied Precision).

Acknowledgments

We are grateful to Tim Bergbrede and the Dortmund Protein Facility for support with vector construction and to all members of the Musacchio laboratory for comments and discussions. K.O. is enrolled in the International Max Planck Research School in Chemical Biology. A.M. acknowledges funding by the European Union's 7th Framework Program ERC agreement KINCON and the Integrated Project MitoSys.

710 **References**

- 711 Bolanos-Garcia, V.M., Lischetti, T., Matak-Vinkovic, D., Cota, E., Simpson, P.J.,
712 Chirgadze, D.Y., Spring, D.R., Robinson, C.V., Nilsson, J., and Blundell, T.L. (2011).
713 Structure of a Blinkin-BUBR1 complex reveals an interaction crucial for kinetochore-
714 mitotic checkpoint regulation via an unanticipated binding Site. *Structure* *19*, 1691–1700.
- 715 Brady, D.M., and Hardwick, K.G. (2000). Complex formation between Mad1p, Bub1p
716 and Bub3p is crucial for spindle checkpoint function. *Curr Biol* *10*, 675–678.
- 717 Caldas, G.V., DeLuca, K.F., and DeLuca, J.G. (2013). KNL1 facilitates phosphorylation
718 of outer kinetochore proteins by promoting Aurora B kinase activity. *J Cell Biol* *203*,
719 957–969.
- 720 Cole, C., Barber, J.D., and Barton, G.J. (2008). The Jpred 3 secondary structure
721 prediction server. *Nucleic Acids Res* *36*, W197–W201.
- 722 Conant, G.C., and Wolfe, K.H. (2008). Turning a hobby into a job: how duplicated genes
723 find new functions. *Nat Rev Genet* *9*, 938–950.
- 724 De Antoni, A., Pearson, C.G., Cimini, D., Canman, J.C., Sala, V., Nezi, L., Mapelli, M.,
725 Sironi, L., Faretta, M., Salmon, E.D., et al. (2005). The Mad1/Mad2 complex as a
726 template for Mad2 activation in the spindle assembly checkpoint. *Current Biology* *15*,
727 214–225.
- 728 Edgar, R.C. (2004). MUSCLE: multiple sequence alignment with high accuracy and high
729 throughput. *Nucleic Acids Res* *32*, 1792–1797.
- 730 Elowe, S., Dulla, K., Uldschmid, A., Li, X., Dou, Z., and Nigg, E.A. (2010). Uncoupling
731 of the spindle-checkpoint and chromosome-congression functions of BubR1. *J Cell Sci*
732 *123*, 84–94.
- 733 Espert A., Uluocak, P., Nunes Bastos, R., Mangat, D., Graab, P., and Gruneberg, U.
734 (2014) PP2A-B56 opposes Mps1 phosphorylation of Knl1 and thereby promotes spindle
735 assembly checkpoint silencing. *J. Cell Biol.* *206*, 833–842.
- 736 Fernius, J., and Hardwick, K.G. (2007). Bub1 kinase targets Sgo1 to ensure efficient
737 chromosome biorientation in budding yeast mitosis. *PLoS Genet* *3*, e213.
- 738 Foley, E.A., and Kapoor, T.M. (2013). Microtubule attachment and spindle assembly
739 checkpoint signalling at the kinetochore. *Nat Rev Mol Cell Biol* *14*, 25–37.
- 740 Foley, E.A., Maldonado, M., and Kapoor, T.M. (2011). Formation of stable attachments
741 between kinetochores and microtubules depends on the B56-PP2A phosphatase. *Nat*
742 *Cell Biol* *13*, 1265–1271.
- 743 Fraschini, R., Beretta, A., Sironi, L., Musacchio, A., Lucchini, G., and Piatti, S. (2001).
744 Bub3 interaction with Mad2, Mad3 and Cdc20 is mediated by WD40 repeats and does
745 not require intact kinetochores. *Embo J* *20*, 6648–6659.
- 746 Gillett, E.S., Espelin, C.W., and Sorger, P.K. (2004). Spindle checkpoint proteins and

747 chromosome-microtubule attachment in budding yeast. *J Cell Biol* *164*, 535–546.

748 Han, J.S., Vitre, B., Fachinetti, D., and Cleveland, D.W. (2014) Bimodal activation of
749 BubR1 by Bub3 sustains mitotic checkpoint signaling. *Proc Natl Acad Sci USA* *111*,
750 E4185-93.

751 Hardwick, K.G., Johnston, R.C., Smith, D.L., and Murray, A.W. (2000). MAD3 encodes
752 a novel component of the spindle checkpoint which interacts with Bub3p, Cdc20p, and
753 Mad2p. *J Cell Biol* *148*, 871–882.

754 Hashimoto, Y., Zhang, S., Zhang, S., Chen, Y.-R., and Blissard, G.W. (2012). Correction:
755 BTI-Tnao38, a new cell line derived from *Trichoplusia ni*, is permissive for AcMNPV
756 infection and produces high levels of recombinant proteins. *BMC Biotechnol.* *12*, 12.

757 Heinrich, S., Windecker, H., Hustedt, N., and Hauf, S. (2012) Mph1 kinetochore
758 localization is crucial and upstream in the hierarchy of spindle assembly checkpoint
759 protein recruitment to kinetochores. *J Cell Sci* *125*, 4720-4727.

760 Hittinger, C.T., and Carroll, S.B. (2007). Gene duplication and the adaptive evolution of a
761 classic genetic switch. *Nature* *449*, 677–681.

762 Howell, B.J., Moree, B., Farrar, E.M., Stewart, S., Fang, G., and Salmon, E.D. (2004).
763 Spindle checkpoint protein dynamics at kinetochores in living cells. *Current Biology* *14*,
764 953–964.

765 Jiang, H., He, X., Wang, S., Jia, J., Wan, Y., Wang, Y., Zeng, R., Yates, J., Zhu, X., and
766 Zheng, Y. (2014). A microtubule-associated zinc finger protein, BuGZ, regulates mitotic
767 chromosome alignment by ensuring Bub3 stability and kinetochore targeting. *Dev Cell*
768 *28*, 268–281.

769 Johnson, V.L., Scott, M.I.F., Holt, S.V., Hussein, D., and Taylor, S.S. (2004). Bub1 is
770 required for kinetochore localization of BubR1, Cenp-E, Cenp-F and Mad2, and
771 chromosome congression. *J Cell Sci* *117*, 1577–1589.

772 Kawashima, S.A., Yamagishi, Y., Honda, T., Ishiguro, K.-I., and Watanabe, Y. (2010).
773 Phosphorylation of H2A by Bub1 Prevents Chromosomal Instability Through Localizing
774 Shugoshin. *Science* *327*, 172–177.

775 Kiyomitsu, T., Obuse, C., and Yanagida, M. (2007). Human Blinkin/AF15q14 is required
776 for chromosome alignment and the mitotic checkpoint through direct interaction with
777 Bub1 and BubR1. *Dev Cell* *13*, 663–676.

778 Klebig, C., Korinth, D., and Meraldi, P. (2009). Bub1 regulates chromosome segregation
779 in a kinetochore-independent manner. *J Cell Biol* *185*, 841–858.

780 Krenn, V., Overlack, K., Primorac, I., van Gerwen, S., and Musacchio, A. (2014). KI
781 Motifs of Human Knl1 Enhance Assembly of Comprehensive Spindle Checkpoint
782 Complexes around MELT Repeats. *Curr Biol* *24*, 29–39.

783 Krenn, V., Wehenkel, A., Li, X., Santaguida, S., and Musacchio, A. (2012). Structural
784 analysis reveals features of the spindle checkpoint kinase Bub1-kinetochore subunit Knl1
785 interaction. *J Cell Biol* *196*, 451–467.

786 Kruse, T., Zhang, G., Larsen, M.S.Y., Lischetti, T., Streicher, W., Kragh Nielsen, T.,
787 Bjørn, S.P., and Nilsson, J. (2013). Direct binding between BubR1 and B56-PP2A
788 phosphatase complexes regulate mitotic progression. *J Cell Sci* 126, 1086–1092.

789 Lampson, M.A., and Kapoor, T.M. (2005). The human mitotic checkpoint protein
790 BubR1 regulates chromosome-spindle attachments. *Nat Cell Biol* 7, 93–98.

791 Lara-Gonzalez, P., Scott, M.I.F., Diez, M., Sen, O., and Taylor, S.S. (2011). BubR1
792 blocks substrate recruitment to the APC/C in a KEN-box-dependent manner. *J Cell Sci*
793 124, 4332–4345.

794 Lara-Gonzalez, P., Westhorpe, F.G., and Taylor, S.S. (2012). The spindle assembly
795 checkpoint. *Curr Biol* 22, R966–R980.

796 Larsen, N.A., Al-Bassam, J., Wei, R.R., and Harrison, S.C. (2007). Structural analysis of
797 Bub3 interactions in the mitotic spindle checkpoint. *Proc Natl Acad Sci USA* 104, 1201–
798 1206.

799 Liu, H., and Naismith, J.H. (2008). An efficient one-step site-directed deletion, insertion,
800 single and multiple-site plasmid mutagenesis protocol. *BMC Biotechnol.* 8, 91.

801 Logarinho, E., Resende, T., Torres, C., and Bousbaa, H. (2008). The human spindle
802 assembly checkpoint protein Bub3 is required for the establishment of efficient
803 kinetochore-microtubule attachments. *Mol Biol Cell* 19, 1798–1813.

804 London, N., and Biggins, S. (2014). Mad1 kinetochore recruitment by Mps1-mediated
805 phosphorylation of Bub1 signals the spindle checkpoint. *Genes Dev* 28, 140–152.

806 London, N., Ceto, S., Ranish, J.A., and Biggins, S. (2012). Phosphoregulation of Spc105
807 by Mps1 and PP1 regulates Bub1 localization to kinetochores. *Curr Biol* 22, 900–906.

808 Luo, X., Tang, Z., Xia, G., Wassmann, K., Matsumoto, T., Rizo, J., and Yu, H. (2004).
809 The Mad2 spindle checkpoint protein has two distinct natively folded states. *Nat Struct*
810 *Mol Biol* 11, 338–345.

811 Malureanu, L.A., Jeganathan, K.B., Hamada, M., Wasilewski, L., Davenport, J., and van
812 Deursen, J.M. (2009). BubR1 N terminus acts as a soluble inhibitor of cyclin B
813 degradation by APC/C(Cdc20) in interphase. *Dev Cell* 16, 118–131.

814 Mapelli, M., Massimiliano, L., Santaguida, S., and Musacchio, A. (2007). The Mad2
815 conformational dimer: structure and implications for the spindle assembly checkpoint.
816 *Cell* 131, 730–743.

817 Meraldi, P., and Sorger, P.K. (2005). A dual role for Bub1 in the spindle checkpoint and
818 chromosome congression. *Embo J* 24, 1621–1633.

819 Millband, D.N.D., and Hardwick, K.G.K. (2002). Fission yeast Mad3p is required for
820 Mad2p to inhibit the anaphase-promoting complex and localizes to kinetochores in a
821 Bub1p-, Bub3p-, and Mph1p-dependent manner. *Mol Cell Biol* 22, 2728–2742.

822 Moyle, M.W., Kim, T., Hattersley, N., Espeut, J., Cheerambathur, D.K., Oegema, K., and
823 Desai, A. (2014). A Bub1-Mad1 interaction targets the Mad1-Mad2 complex to

unattached kinetochores to initiate the spindle checkpoint. *J Cell Biol*.

Musacchio, A., and Salmon, E.D. (2007). The spindle-assembly checkpoint in space and time. *Nat Rev Mol Cell Biol* 8, 379–393.

Nijenhuis, W., Castelmur, von, E., Littler, D., De Marco, V., Tromer, E., Vleugel, M., van Osch, M.H.J., Snel, B., Perrakis, A., and Kops, G.J.P.L. (2013). A TPR domain-containing N-terminal module of MPS1 is required for its kinetochore localization by Aurora B. *J Cell Biol* 201, 217–231.

Nijenhuis, W., Vallardi, G., Teixeira, A., Kops, G.J.P.L., and Saurin, A.T. (2014). Negative feedback at kinetochores underlies a responsive spindle checkpoint signal. *Nat Cell Biol* 16, 1257–1264.

Overlack, K., Krenn, V., and Musacchio, A. (2014). When Mad met Bub. *Nature Publishing Group* 15, 326–328.

Perera, D., Tilston, V., Hopwood, J.A., Barchi, M., Boot-Handford, R.P., and Taylor, S.S. (2007). Bub1 maintains centromeric cohesion by activation of the spindle checkpoint. *Dev Cell* 13, 566–579.

Primorac, I., Weir, J.R., Chirolì, E., Gross, F., Hoffmann, I., van Gerwen, S., Ciliberto, A., and Musacchio, A. (2013). Bub3 reads phosphorylated MELT repeats to promote spindle assembly checkpoint signaling. *eLife* 2, e01030.

Rischitor, P.E.P., May, K.M.K., and Hardwick, K.G.K. (2006). Bub1 is a fission yeast kinetochore scaffold protein, and is sufficient to recruit other spindle checkpoint proteins to ectopic sites on chromosomes. *PLoS ONE* 2, e1342–e1342.

Santaguida, S., Tighe, A., D'Alise, A.M., Taylor, S.S., and Musacchio, A. (2010). Dissecting the role of MPS1 in chromosome biorientation and the spindle checkpoint through the small molecule inhibitor reversine. *J Cell Biol* 190, 73–87.

Shah, J.V., Botvinick, E., Bonday, Z., Furnari, F., Berns, M., and Cleveland, D.W. (2004). Dynamics of centromere and kinetochore proteins; implications for checkpoint signaling and silencing. *Curr Biol* 14, 942–952.

Sharp-Baker, H., and Chen, R.H. (2001). Spindle checkpoint protein Bub1 is required for kinetochore localization of Mad1, Mad2, Bub3, and CENP-E, independently of its kinase activity. *J Cell Biol* 153, 1239–1250.

Shepperd, L.A.L., Meadows, J.C.J., Sochaj, A.M.A., Lancaster, T.C.T., Zou, J.J., Buttrick, G.J.G., Rappsilber, J.J., Hardwick, K.G.K., and Millar, J.B.A.J. (2012). Phosphodependent recruitment of Bub1 and Bub3 to Spc7/KNL1 by Mph1 kinase maintains the spindle checkpoint. *Current Biology* 22, 891–899.

Simonetta, M., Manzoni, R., Mosca, R., Mapelli, M., Massimiliano, L., Vink, M., Novak, B., Musacchio, A., and Ciliberto, A. (2009). The influence of catalysis on mad2 activation dynamics. *PLoS Biol* 7, e10.

Sudakin, V., Chan, G.K., and Yen, T.J. (2001). Checkpoint inhibition of the APC/C in HeLa cells is mediated by a complex of BUBR1, BUB3, CDC20, and MAD2. *J Cell Biol*

863 154, 925–936.

864 Suijkerbuijk, S.J.E., van Dam, T.J.P., Karagöz, G.E., Castelmur, von, E., Hubner, N.C.,
865 Duarte, A.M.S., Vleugel, M., Perrakis, A., Rüdiger, S.G.D., Snel, B., et al. (2012a). The
866 Vertebrate Mitotic Checkpoint Protein BUBR1 Is an Unusual Pseudokinase. *Dev Cell* 22,
867 1321–1329.

868 Suijkerbuijk, S.J.E., Vleugel, M., Teixeira, A., and Kops, G.J.P.L. (2012b). Integration of
869 Kinase and Phosphatase Activities by BUBR1 Ensures Formation of Stable
870 Kinetochore-Microtubule Attachments. *Dev Cell* 23, 745–755.

871 Taylor, S.S., Ha, E., and McKeon, F. (1998). The human homologue of Bub3 is required
872 for kinetochore localization of Bub1 and a Mad3/Bub1-related protein kinase. *J Cell Biol*
873 142, 1–11.

874 Toledo, C.M., Herman, J.A., Olsen, J.B., Ding, Y., Corrin, P., Girard, E.J., Olson, J.M.,
875 Emili, A., DeLuca, J.G., and Paddison, P.J. (2014). BuGZ is required for Bub3 stability,
876 Bub1 kinetochore function, and chromosome alignment. *Dev Cell* 28, 282–294.

877 Trowitzsch, S., Bieniossek, C., Nie, Y., Garzoni, F., and Berger, I. (2010). New
878 baculovirus expression tools for recombinant protein complex production. *J Struct Biol*
879 172, 45–54.

880 Vanoosthuyse, V., Valsdottir, R., Javerzat, J.-P., and Hardwick, K.G. (2004). Kinetochore
881 targeting of fission yeast Mad and Bub proteins is essential for spindle checkpoint
882 function but not for all chromosome segregation roles of Bub1p. *Mol Cell Biol* 24, 9786–
883 9801.

884 Vleugel, M., Hoogendoorn, E., Snel, B., and Kops, G.J.P.L. (2012). Evolution and
885 Function of the Mitotic Checkpoint. *Dev Cell* 23, 239–250.

886 Vleugel, M., Tromer, E., Omerzu, M., Groenewold, V., Nijenhuis, W., Snel, B., and Kops,
887 G.J.P.L. (2013). Arrayed BUB recruitment modules in the kinetochore scaffold KNL1
888 promote accurate chromosome segregation. *J Cell Biol* 203, 943–955.

889 Wang, F., Ulyanova, N.P., van der Waal, M.S., Patnaik, D., Lens, S.M.A., and Higgins,
890 J.M.G. (2011). A positive feedback loop involving Haspin and Aurora B promotes CPC
891 accumulation at centromeres in mitosis. *Curr Biol* 21, 1061–1069.

892 Xu, P., Raetz, E.A., Kitagawa, M., Virshup, D.M., and Lee, S.H. (2013). BUBR1 recruits
893 PP2A via the B56 family of targeting subunits to promote chromosome congression.
894 *Biol Open* 2, 479–486.

895 Yamagishi, Y., Yang, C.-H., Tanno, Y., and Watanabe, Y. (2012). MPS1/Mph1
896 phosphorylates the kinetochore protein KNL1/Spc7 to recruit SAC components. *Nat*
897 *Cell Biol* 14, 746–752.

898

Figure legends

Figure 1 *Mps1 and Bub1 are required for kinetochore localization of BubR1*

A) Similar domain organization of the homologous proteins Bub1 and BubR1. TPR – tetra-tricopeptide repeat, B3BD – Bub3 binding domain, B1 – Bub1, BR1 – BubR1. **B)** Schematic depiction of the outer KT (KMN network). MELT repeats of Knl1 are phosphorylated by the checkpoint kinase Mps1 and recruit Bub1/Bub3 to KTs. It is not clear how BubR1 is recruited to KTs. **C-D)** Quantitative IP-mass spectrometry analyses showing that the interaction of Bub1, BubR1 and Bub3 with KTs is significantly reduced upon inhibition of Mps1 with Reversine. Green- and red-labeled hits indicate respectively proteins whose levels were not strongly affected or were strongly affected in the presence of Reversine. **E and G)** Representative images of Flp-In T-REx cell lines in BubR1 (**E**) and Bub1 (**G**) RNAi, respectively, after treatment with nocodazole, showing that Bub1 is required for BubR1 KT localization. Scale bar: 10 μ m. **F and H)** Quantification of Bub1 and BubR1 KT levels, respectively, in cells treated as in panel **E** and **G**. The graph shows mean intensity, error bars indicate SD. The mean value for non-depleted cells is set to 1. **I-J)** Representative images of stable Flp-In T-REx cell lines expressing the indicated GFP-Bub1 constructs (panel **I**) or HeLa cells transfected with the indicated GFP-BubR1 constructs (panel **J**) after treatment with nocodazole. The same images are also shown in Figures 4A and Figure 5C, and quantified in Figures 4B and 5B. Scale bar: 10 μ m.

Figure 2 *The loop regions of Bub1 and BubR1 modulate the interaction of Bub3 with phosphorylated MELT motifs*

A) Recombinant Bub3, Bub1²⁰⁹⁻²⁷⁰/Bub3 and BubR1³⁶²⁻⁴³¹/Bub3 were incubated with immobilized MBP-Knl1^{MELT1} (residues 138-168 of human Knl1) prephosphorylated with Mps1 (+) or unphosphorylated (-). Empty lanes (-) demonstrate lack of background binding to empty beads. wt – wild type; B3 – Bub3; B1 – Bub1; BR1 – BubR1. **B)** Multiple sequence alignments of the Bub3 binding domains (B3BD) of human (*Homo sapiens*, Hs), chicken (*Gallus gallus*, gg), frog (*Xenopus laevis*, Xl) and budding yeast (*Saccharomyces cerevisiae*, Sc) Bub1 and BubR1s. Mad3 is the budding yeast BubR1 homolog. ScBub1^{R314} (red asterisk) directly contributes to the interaction with the MELT^p peptide. The different Bub1 and BubR1 sequences were aligned manually on the basis of the crystal structures of the B3BDs of Mad3 and Bub1 in complex with Bub3

(Larsen et al., 2007; Primorac et al., 2013)). **C)** Crystal structure of the ScBub1²⁸⁹⁻³⁵⁹-Bub3-MELT^P ternary complex (Primorac et al., 2013). N and C indicate the N- and C-terminus, respectively. **D)** Close-up of the MELT^P binding site indicating the role of ScBub1^{R314} in MELT^P binding. **E)** Schematic depiction of short Bub1 and BubR1 “loopswap” constructs, containing the loop (different shades of red) followed by the Bub3-binding domain (different shades of yellow). **F)** Recombinant BubR1³⁶²⁻⁴³¹/Bub3 with its own loop (wt) or with the Bub1 loop (B1) and recombinant Bub1²⁰⁹⁻²⁷⁰/Bub3 with its own loop (wt) or with the BubR1 loop (BR1) were incubated with immobilized MBP-Knl1^{MELT¹} prephosphorylated with Mps1 (+) or unphosphorylated (-) as in panel A. Empty lanes (-) demonstrate lack of background binding to empty beads. **G)** Western Blot of immunoprecipitates (IP) from mitotic Flp-In T-REx cell lines expressing the indicated GFP-Bub1 and -BubR1 constructs showing the influence of the loop on the ability to pull down the KT-components Knl1 and Mis12. Tubulin was used as loading control. **H)** Quantification of the Western Blot in (G). In the upper graph the amounts of co-precipitating BubR1, Bub3, Knl1 and Mis12 were normalized to the amount of GFP-Bub1 bait present in the IP. In the lower graph the amounts of co-precipitating Bub1, Bub3, Knl1 and Mis12 were normalized to the amount of GFP-BubR1 bait. Values for GFP-Bub1 wt and GFP-BubR1 wt, respectively are set to 1. The graphs show mean intensity of two independent experiments (for Mis12 only one). Error bars represent SD.

Figure 3 Behavior of the “loop swap” mutants in HeLa cells

A) Representative images of stable Flp-In T-REx cells expressing either GFP-Bub1 wild type (wt) or the loop mutant showing that the BR1-loop impairs KT localization. Scale bar: 10 µm. **B)** Quantification of Bub1 KT levels in cells treated as in panel A. The graph shows mean intensity from three independent experiments. Error bar represents SEM. Values for Bub1 wt are set to 1. **C)** Representative images of stable Flp-In T-REx cells expressing either GFP-BubR1 wt or the loopmutant showing that the B1-loop enhances KT localization. Scale bar: 10 µm. **D)** Quantification of BubR1 KT levels in cells treated as in panel C. The graph shows mean intensity from three independent experiments. Error bar represents SEM. Values for BubR1 wt are set to 1. **E)** Representative images of HeLa cells transfected with the indicated GFP-BubR1 constructs, showing that

BubR1 B1-loop is independent of Bub1 for its KT localization. In brief, after transfection, cells were depleted of endogenous Bub1 by RNAi, synchronized with a double thymidine block and arrested in mitosis with nocodazole. Scale bar: 10 μ m. **F)** Quantification of BubR1 KT levels in cells treated as in panel E. The graph shows mean intensity from three independent experiments. Error bars represent SEM. Values for BubR1^{wt} in non-depleted cells are set to 1. **G)** Representative images of HeLa cells transfected with GFP-BubR1 B1-loop treated as in panel E in the presence (+) or absence (-) of the Mps1 inhibitor Reversine, showing that BubR1 B1-loop KT localization is dependent on Mps1. Scale bar: 10 μ m. **H)** Quantification of BubR1 KT levels in cells treated as in panel G. The graph shows mean intensity from two independent experiments. Error bars represent SEM. Values for BubR1^{wt} in non-depleted cells without Reversine (images are shown in Figure 3 Supplement 1, panel A) are set to 1. **I)** Mean duration of mitosis of Flp-In T-REx stable cell lines expressing GFP-BubR1 wt or the loop mutant in the absence of endogenous BubR1 and in the presence of 50 nM nocodazole. Cell morphology was used to measure entry into and exit from mitosis by time-lapse-microscopy (n>58 per cell line) from three independent experiments. Error bars depict SEM. **J)** Western Blot of immunoprecipitates (IP) from mitotic Flp-In T-REx cell lines expressing the indicated GFP-BubR1 constructs showing the influence of the loop on the ability to pull down MCC and APC/C components. Tubulin was used as loading control. **K)** Western Blot of immunoprecipitates (IP) of the APC/C subunit Cdc27 from mitotic Flp-In T-REx cell lines expressing the indicated GFP-BubR1 constructs showing the influence of the loop on the incorporation into APC/C-bound MCC. Tubulin was used as loading control.

Figure 4 A minimal BubR1-binding region of Bub1

A and **C)** Representative images of stable Flp-In T-REx cell lines expressing the indicated GFP-Bub1 constructs after treatment with nocodazole, showing that Bub1²⁰⁹⁻⁴⁰⁹ is sufficient to recruit BubR1 (panel **A**) and that residues 271-409 are essential for this function (panel **C**). Scale bar: 10 μ m. **B** and **D)** Quantification of BubR1 KT levels in cells treated as in panels B and D, respectively. The graphs show mean intensity of two independent experiments, the error bars indicate SEM. The mean value for non-depleted cells expressing GFP (panel **B**) or GFP-Bub1²⁰⁹⁻⁴⁰⁹ (panel **D**) is set to 1. **E)** Western blot of immunoprecipitates (IP) from mitotic Flp-In T-REx cell lysates expressing the

indicated GFP-Bub1 constructs in the presence or absence of endogenous Bub1, showing that Bub1²⁰⁹⁻⁴⁰⁹ is sufficient to pull down BubR1. Tubulin was used as loading control. **F)** Quantification of the Western Blot in panel E. The amounts of co-precipitating BubR1, Bub3 and Knl1 were normalized to the amount of GFP-Bub1 bait present in the IP. Values for GFP-Bub1 FL in non-depleted cells are set to 1. The graph shows mean intensity of two independent experiments. Error bars represent SD. **G)** BubR1¹⁻⁵⁷¹/Bub3 and Bub1¹⁻⁴⁰⁹/Bub3 interact in size exclusion chromatography, which separates proteins based on size and shape. H6 and TRX are tags used for protein purification and expression. **H)** BubR1¹⁻⁵⁷¹ and Bub1¹⁻⁴⁰⁹/Bub3 interact in size exclusion chromatography. **I)** BubR1¹⁻⁵⁷¹/Bub3 and Bub1²⁰⁹⁻⁴⁰⁹/Bub3 interact in size exclusion chromatography. **J)** BubR1¹⁻⁵⁷¹/Bub3 and Bub1²⁷¹⁻⁴⁰⁹ do not interact in size exclusion chromatography. MBP – maltose binding protein, mAu – milliabsorbance unit.

Figure 5 A minimal Bub1-binding region of BubR1

A and C) Representative images of HeLa cells transfected with the indicated GFP-BubR1 constructs. Cells were treated as described in Figure 3E. BubR1³⁶²⁻⁵⁷¹ is the minimal construct that is able to localize to KT's in presence of Bub1. Scale bar: 10 μ m. **B)** Quantification of BubR1 KT levels in cells treated as in panels A and C. The graph shows mean intensity of at least two independent experiments, error bars depict SEM. Values for GFP-BubR1 FL in non-depleted cells are set to 1. **D)** BubR1³⁶²⁻⁵⁷¹ and Bub1¹⁻⁴⁰⁹/Bub3 interact in size exclusion chromatography. **E)** BubR1³⁶²⁻⁴³¹/Bub3 and Bub1¹⁻⁴⁰⁹/Bub3 do not interact in size exclusion chromatography. **F)** BubR1⁴³²⁻⁵⁷¹ and Bub1¹⁻⁴⁰⁹/Bub3 do not interact in size exclusion chromatography. mAU – milliabsorbance unit.

Figure 6 A pseudo-symmetric Bub1-BubR1 interaction

A) The identified minimal constructs BubR1³⁶²⁻⁵⁷¹ and Bub1²⁰⁹⁻⁴⁰⁹/Bub3 interact in size exclusion chromatography. **B)** Summary of the behavior of the indicated Bub1 and BubR1 constructs. **C and E)** Representative images of HeLa cells transfected with the indicated GFP-BubR1 constructs showing that neither BubR1 ^{Δ 432-484} (panel C), which lacks the predicted helical segment of the C-terminal extension, nor BubR1^{E409K+E413K} (panel E), which is not able to bind Bub3, are able to localize to KT's. Cells were treated

as in Figure 3E. For BubR1^{Δ432-484} two different expression levels are depicted in the non-depleted condition. Scale bar: 10 μm. **D** and **F**) Quantification of BubR1 KT levels in cells treated as in panels C and E, respectively. The graph shows mean intensity from at least two independent experiments. Error bars represent SEM. Values for BubR1^{FL} in non-depleted cells are set to 1. **G**) Domain organization of LacI-GFP-Bub1 constructs. **H**) LacI-Bub1^{wt} recruits BubR1 to the Lac-Operator, whereas Bub1^{E252K}, which cannot bind Bub3, does not.

Figure 7 *Functional characterization of BubR1 mutants*

A) Mean duration of mitosis of Flp-In T-REx stable cell lines expressing GFP-BubR1 wt or the indicated mutants in the absence of endogenous BubR1 and in the presence of 50 nM nocodazole. Cell morphology was used to measure entry into and exit from mitosis by time-lapse-microscopy (n>44 per cell line per experiment) from at least three independent experiments. Error bars depict SEM. **B**) Western Blot of immunoprecipitates (IP) from mitotic Flp-In T-REx cell lines expressing the indicated GFP-BubR1 constructs. Tubulin was used as loading control. **C**) Quantification of the Western Blot in Figure 7B. The amounts of co-precipitating proteins were normalized to the amount of GFP-BubR1 bait present in the IP. Values for GFP-BubR1 wt are set to 1. The graphs show mean intensity of two independent experiments. Error bars represent SEM. **D**) Analysis of cold-stable microtubules in cells expressing the indicated GFP-BubR1. **E**) Western Blot of immunoprecipitates (IP) from mitotic Flp-In T-REx cell lines expressing the indicated GFP-BubR1 constructs. The asterisk represents an unspecific band recognized by the PP2A antibody.

Figure 8 *Extension of the template model*

A) Model of the Bub1-BubR1 interaction. The upper part shows the described KT recruitment mechanism of BubR1/Bub3, which in turn recruits the phosphatase PP2A, to a Bub1/Bub3 complex on Knl1. The lower part depicts a close-up of the identified pseudo-symmetric Bub1-BubR1 interaction, which involves equivalent segments of Bub1 and BubR1 comprising the Bub3 binding domain and a C-terminal extension whose first part is predicted to have a helical fold in both proteins. The presence of Bub3 on both

proteins seems to be essential for this interaction, although due to different reasons (for more explanations see text). The TPR regions of human Bub1 and BubR1 bind to non-conserved short motifs of Knl1 named KI1 and KI2, respectively (Kiyomitsu et al., 2007; Krenn et al., 2012; 2014). **B)** Extension of the template model. Mad1/C-Mad2 at KT's is known to act as a template for the establishment of the Cdc20/C-Mad2 interaction. This seems similar to the BubR1 recruitment mechanism, wherein Bub1/Bub3 recruits BubR1/Bub3 through a pseudo-symmetric interaction. Ultimately, the entire MCC (BubR1/Bub3 and Cdc20/C-Mad2) may represent the copy of a KT template consisting of Bub1/Bub3 and Mad1/C-Mad2.

Legends of Figure Supplements

Figure 1 Supplement 1 *RNAi quantification and schematic depiction of Bub1 and BubR1 constructs A-B*) Quantification of RNAi-based depletion of Bub1 and BubR1. Shown are mean and standard deviation from two independent experiments. **C-D**) Schematic depiction of the main Bub1 and BubR1 deletion constructs used in this study. TPR, tetratricopeptide repeats; B3BD, Bub3 binding domain; BR1, BubR1; FL, full-length; N, N-terminus.

Figure 2 Supplement 1 *Validation of recombinant “loopswap” mutants*

The indicated constructs were purified and separated by SDS-PAGE after purification. Both wild type and chimeric constructs interact normally and with similar affinity with Bub3.

Figure 3 Supplement 1 *Additional characterization of “loopswap” mutants*

A) Representative images of HeLa cells transfected with GFP-BubR1^{wt} treated as in Figure 3E in the presence (+) or absence (-) of the Mps1 inhibitor Reversine as control for the experiment shown in Figure 3G. The corresponding quantification is shown in Figure 3H. Scale bar: 10 μ m. **B)** Quantification of Bub1 kinetochore levels in cells treated as in Figure 3E. The graph shows mean intensity from three independent experiments. Error bars represent SEM. Values for Bub1 in BubR1^{wt} expressing cells are set to 1. **C)** Quantification of the Western Blot in Figure 3J. The amounts of co-precipitating MCC and APC/C components were normalized to the amount of GFP-BubR1 bait present in the IP. Values for GFP-BubR1 wt are set to 1. The graphs show mean intensity of two independent experiments. Error bars represent SEM. **D)** Quantification of the Western Blot in Figure 3K. The amounts of co-precipitating proteins were normalized to the amounts present in GFP-BubR1 wt expressing cells. The graphs show mean intensity of two independent experiments. Error bars represent SEM.

Figure 4 Supplement 1 *Additional chromatographic experiments*

A) BubR1¹⁻⁵⁷¹ and Bub1²⁰⁹⁻⁴⁰⁹/Bub3 interact in size exclusion chromatography. **B)** BubR1¹⁻⁵⁷¹/Bub3 and Bub1²⁰⁹⁻²⁷⁰/Bub3 do not interact in size exclusion chromatography. The control run of Bub1²⁰⁹⁻²⁷⁰/Bub3 is missing due to limiting amounts of the protein. **C)** BubR1²²²⁻⁵⁷¹/Bub3 and Bub1¹⁻²⁸⁰/Bub3 do not interact in size exclusion chromatography. **D)** BubR1²²²⁻⁵⁷¹/Bub3 and Bub1¹⁻⁴⁰⁹/Bub3 interact in size exclusion chromatography. mAU – milliabsorbance unit.

Figure 4 Supplement 2 *The TPR domain of Bub1 influences KT binding affinity in addition to the loop region*

A) Representative images of HeLa cells transfected with the indicated GFP-Bub1^{FL} constructs, showing that the BR1-loop impairs KT localization. However in the absence of endogenous Bub1 considerable binding affinity is regained. Cells were treated as described in Figure 3E. Scale bar: 10 µm. **B)** Representative images of HeLa cells transfected with the indicated GFP-Bub1²⁰⁹⁻⁴⁰⁹ constructs, showing that this construct, which lacks the N-terminal TPR domain, does not regain considerable binding affinity in the absence of Bub1. Cells were treated as described in Figure 3E. Scale bar: 10 µm. **C)** Representative images of HeLa cells transfected with the indicated GFP-Bub1¹⁻⁴⁰⁹ constructs, showing that the TPR domain is contributing to regaining KT binding affinity in the absence of endogenous Bub1. Cells were treated as described in Figure 3E. Scale bar: 10 µm. **D)** Quantification of Bub1 KT levels in cells treated as in panels A-C. The graph shows mean intensity from two independent experiments. Error bars represent SEM. Values for Bub1^{FL} in non-depleted cells were set to 1.

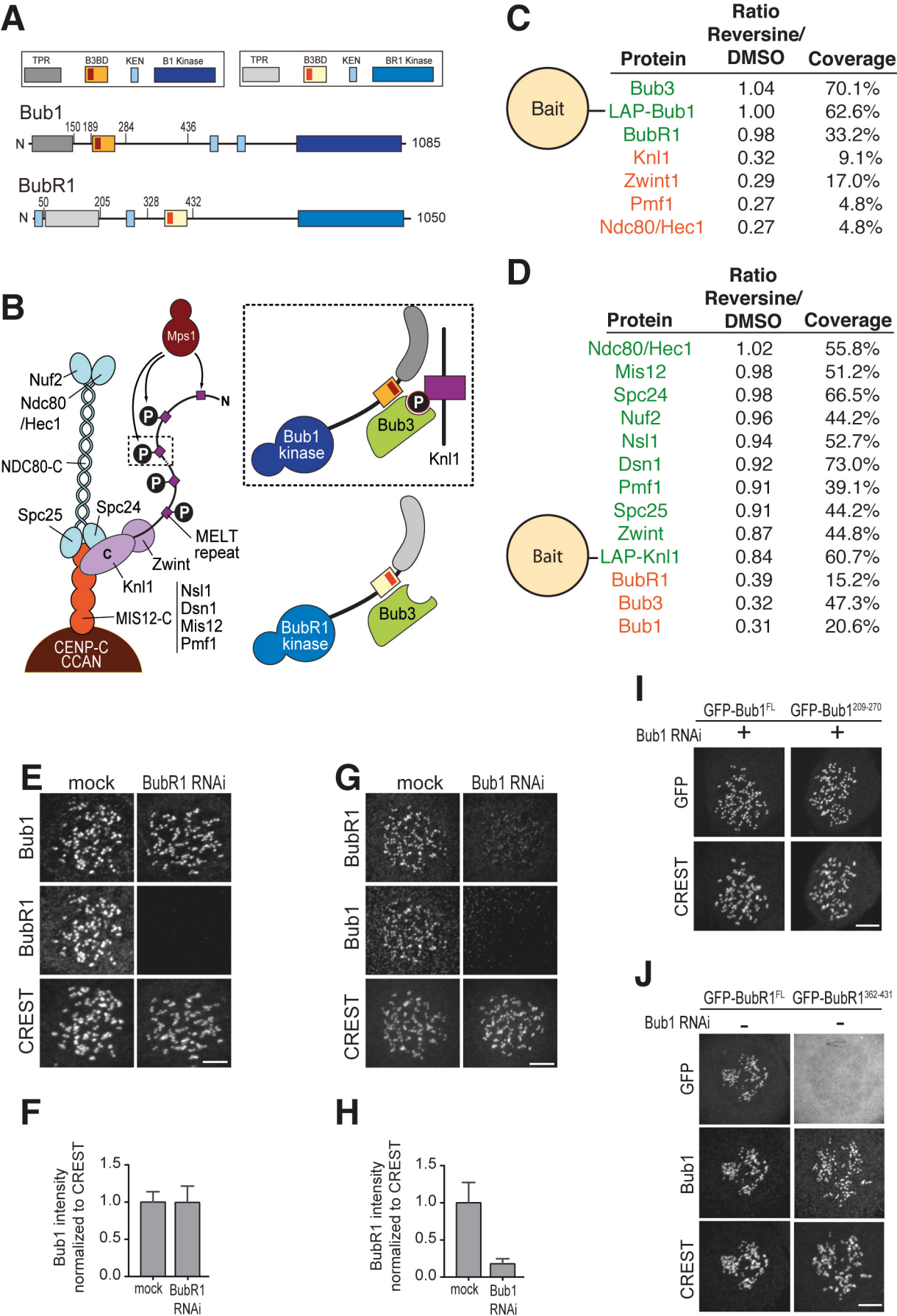
Figure 4 Supplement 3 *The TPR domain of BubR1 influences kinetochore binding affinity in addition to the loop region*

A) Representative images of HeLa cells transfected with the indicated GFP-BubR1³⁶²⁻⁵⁷¹ constructs, showing that the B1-loop enhances kinetochore localization. However in the absence of endogenous Bub1 the short loop mutant, which lacks the N-terminal TPR domain, is less efficient than the full length BubR1 in its localization to kinetochores (Figure 3E). Cells were treated as described in Figure 3E. Scale bar: 10 µm. **B)** Representative images of HeLa cells transfected with the indicated GFP-BubR1¹⁻⁵⁷¹ constructs, showing that the TPR domain is contributing together with the loop region

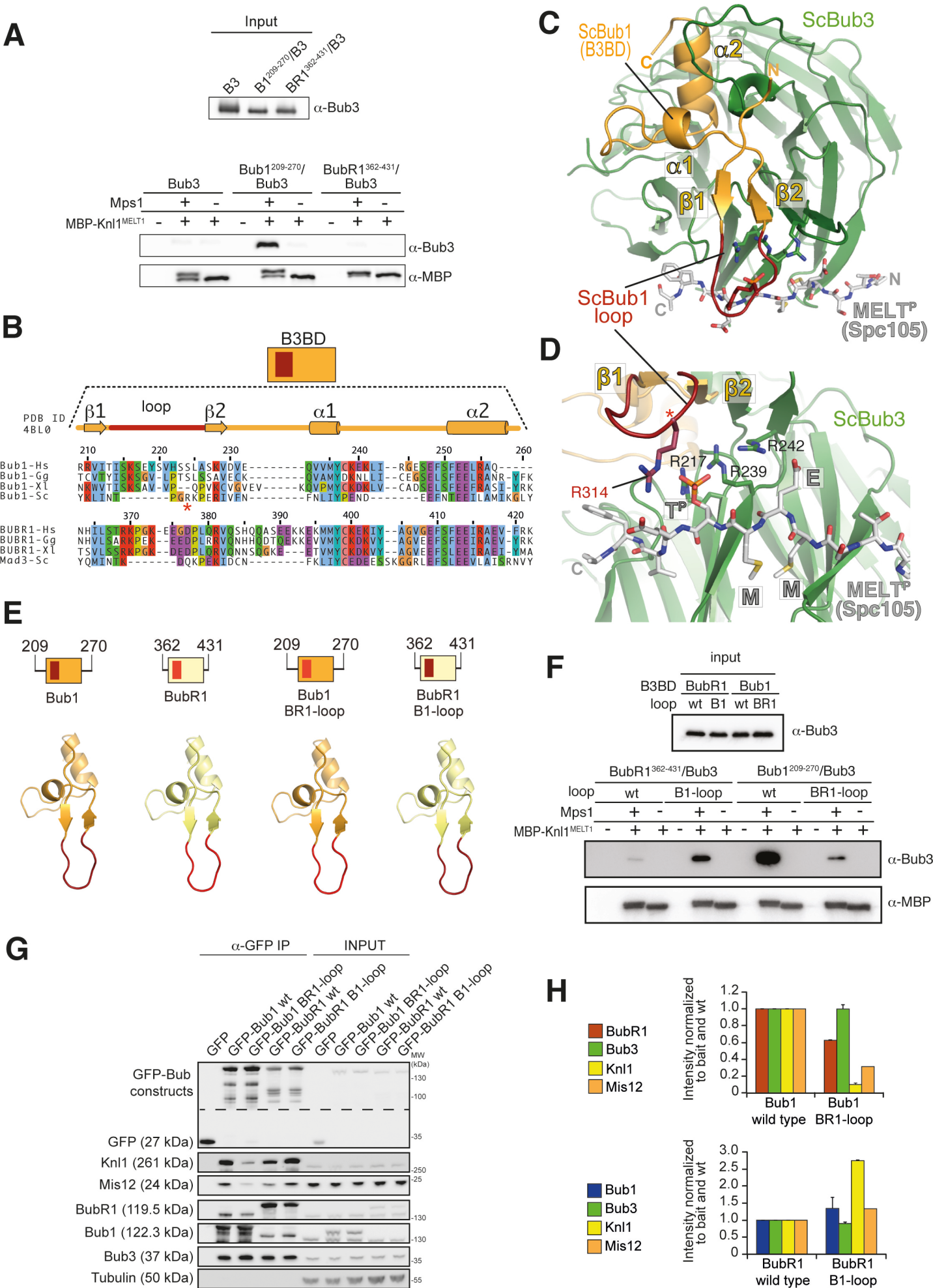
to the ability to stay at KT's in the absence of endogenous Bub1. Cells were treated as described in Figure 3E. Scale bar: 10 μ m. **C)** Quantification of BubR1 KT levels in cells treated as in (A-B). The graph shows mean intensity from at least two independent experiments. Error bars represent SEM. Values for BubR1^{FL} in non-depleted cells are set to 1.

Figure 6 Supplement 1 *Alignment of the Bub1 and BubR1 interaction domains*

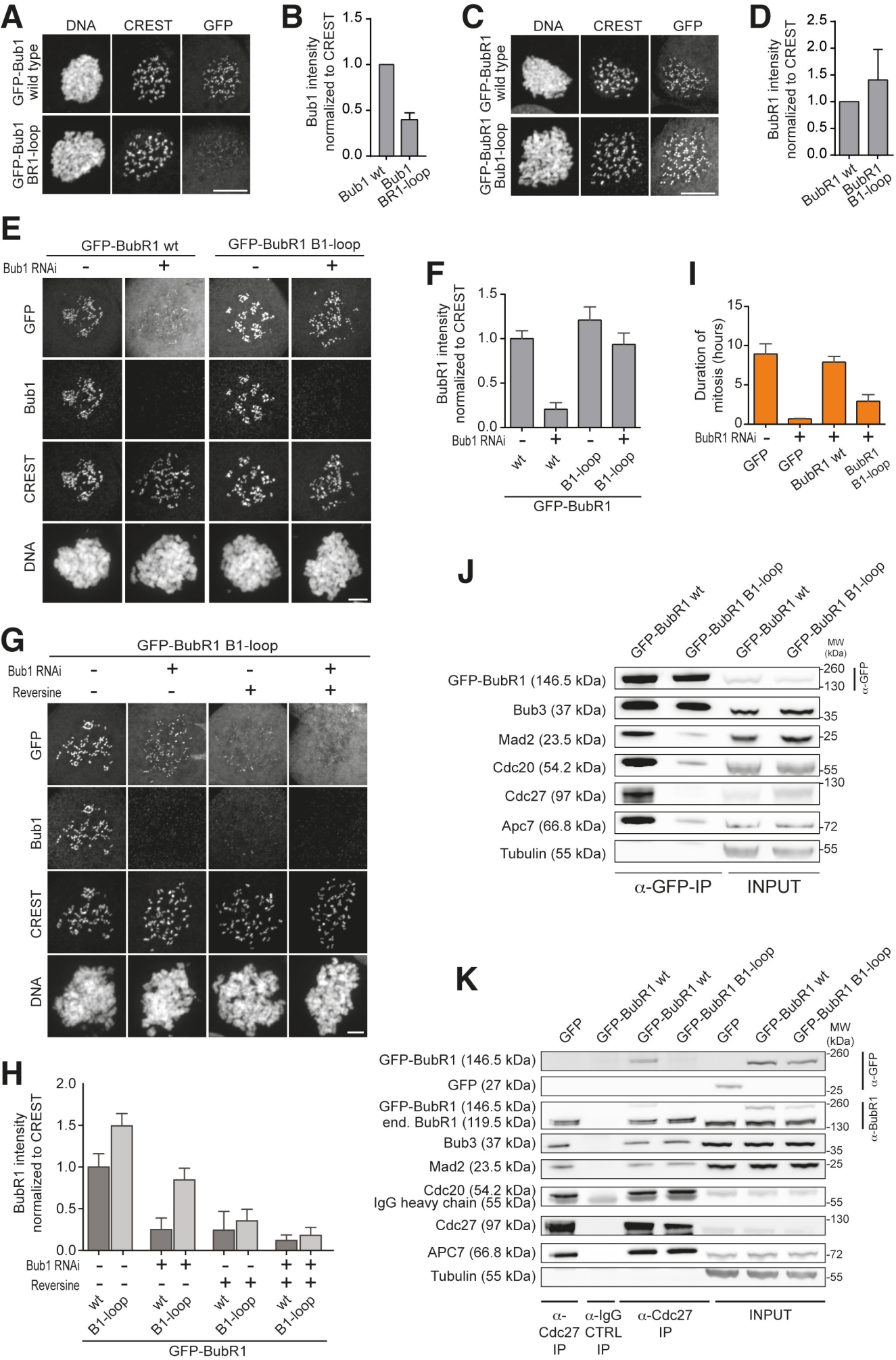
A) Multiple sequence alignments of the interacting domains of Bub1 and BubR1 from four different species (*Homo sapiens*, Hs), chicken (*Gallus gallus*, Gg), frog (*Xenopus laevis*, Xl) and budding yeast (*Saccharomyces cerevisiae*, Sc). Mad3 is the budding yeast BubR1 homolog. **B)** Representative images of HeLa cells transfected with the indicated GFP-BubR1 constructs, showing that also the short Bub3 binding domain mutant is not able to localize to KT's. Cells were treated as described in Figure 3E. Scale bar: 10 μ m. **C)** Quantification of BubR1 KT levels in cells treated as in panel **B**. The graph shows mean intensity from two independent experiments. Error bars represent SEM. Values for BubR1³⁶²⁻⁵⁷¹ in non-depleted cells are set to 1. **D)** Quantification of co-localization. Data represent normalized mean intensities and standard deviations from 12 cells. BubR1 was identified at the ectopic locus on 12/12 cells for the wild type and on 0/12 cells for the E252K mutant.



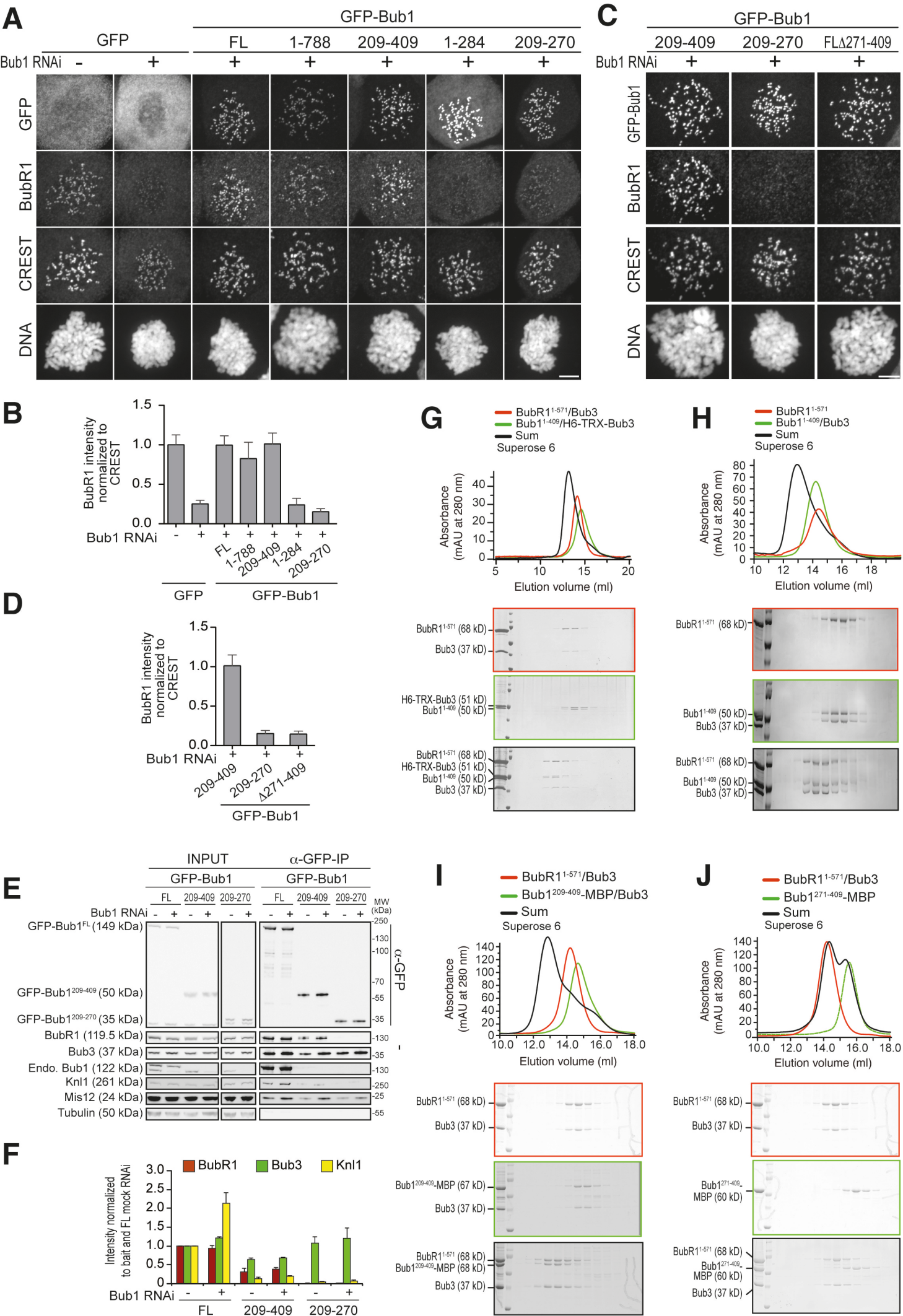
Overlack, Primorac et al.
Figure 1

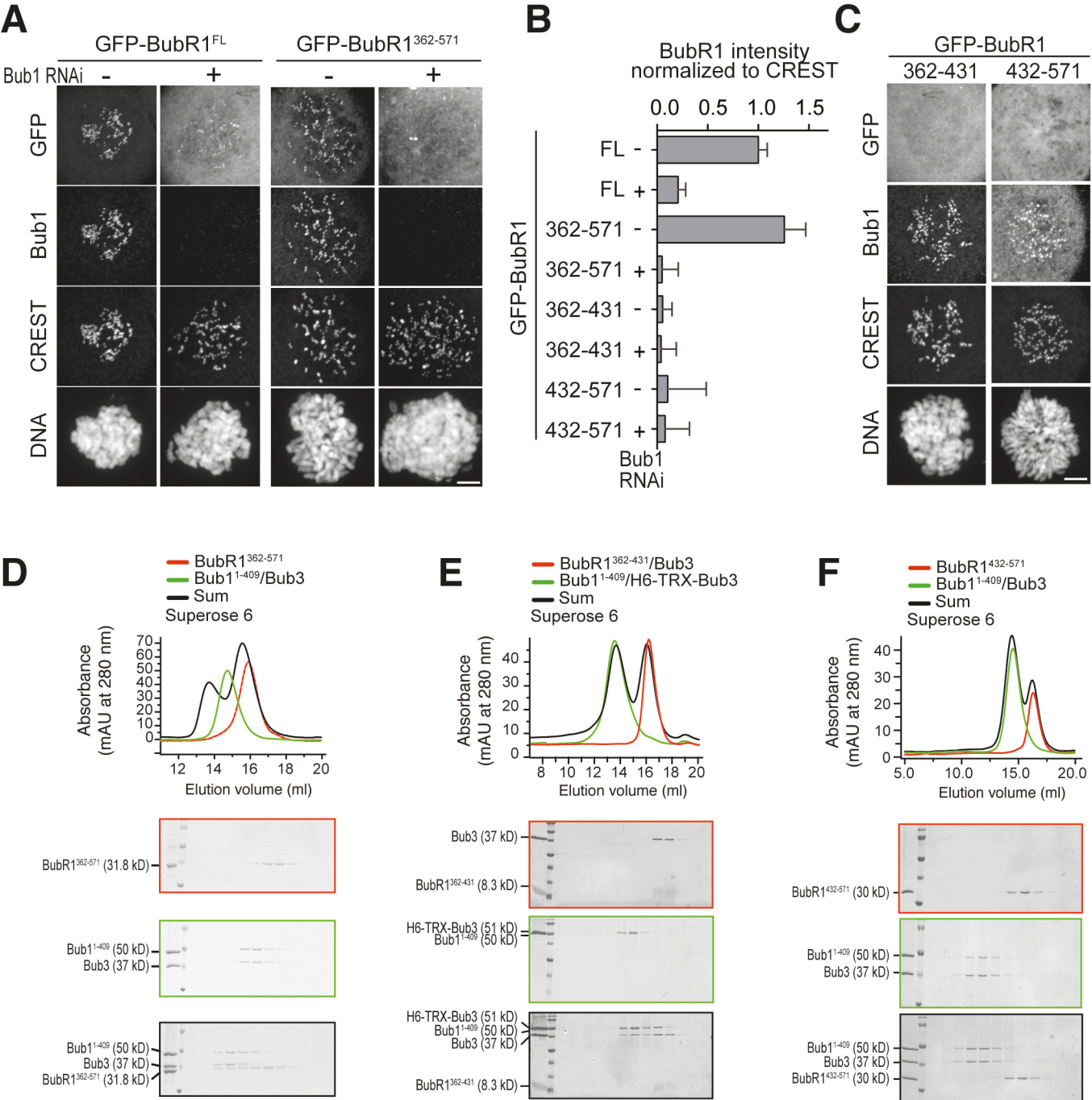


Overlack, Primorac et al.
Figure 2

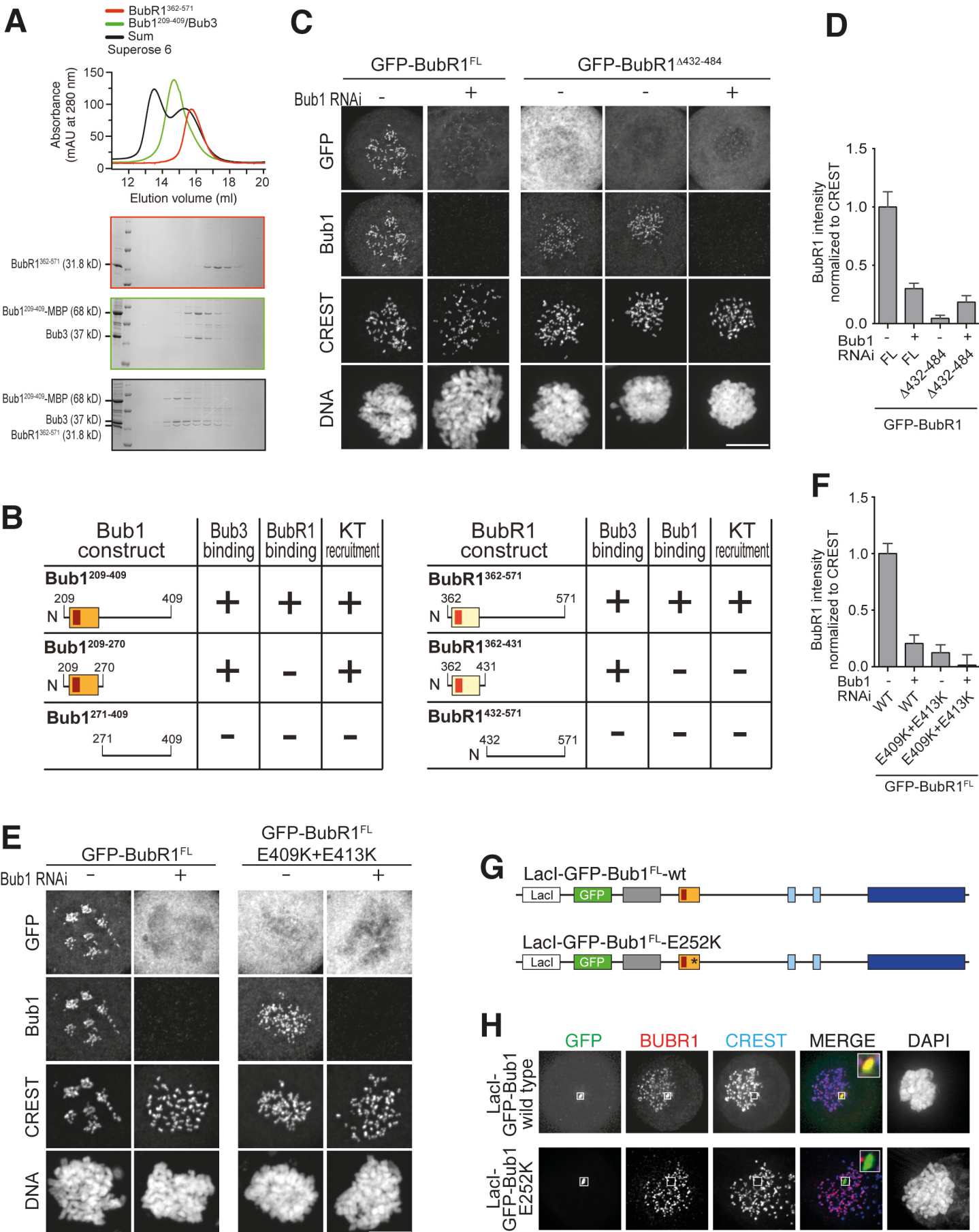


Overlack, Primorac et al.
Figure 3

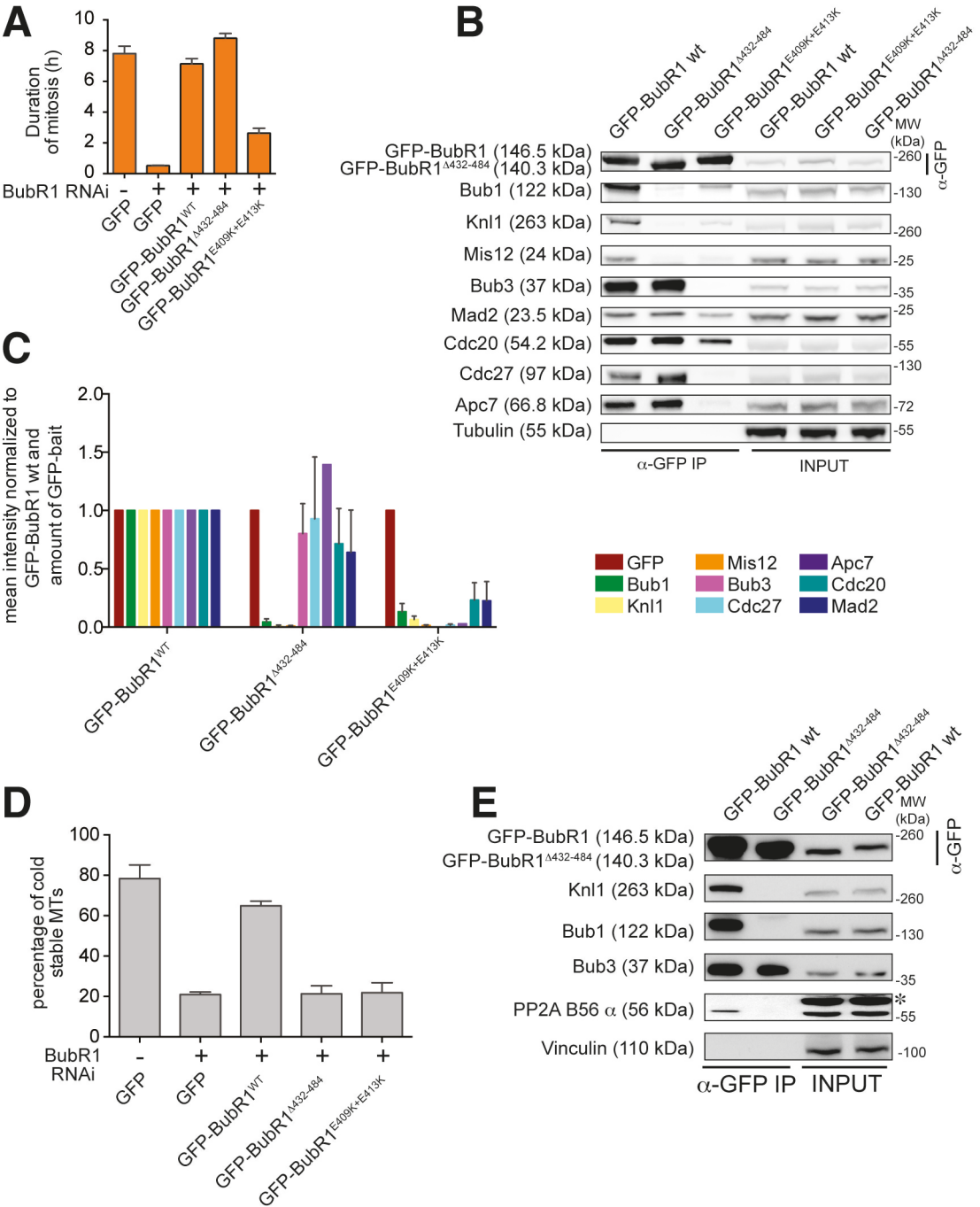




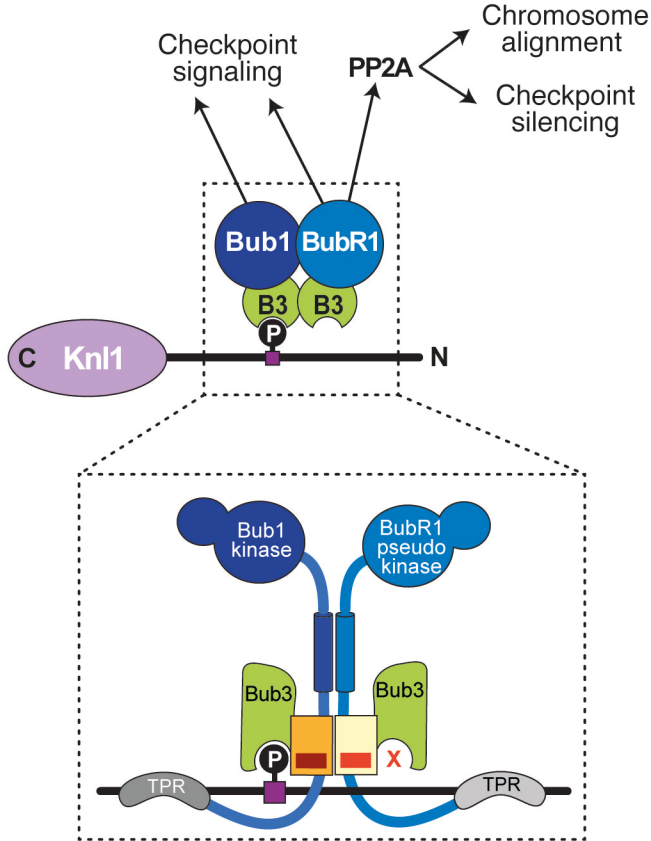
Overlack, Primorac et al.
Figure 5



Overlack, Primorac et al.
Figure 6



Overlack, Primorac et al.
Figure 7

A**B**